TRW REPORT NO. 14103-6002-R0-00

APTD-1065

PB 209 886

INVESTIGATION OF SCATTERED LIGHT HOLOGRAPHY OF AEROSOLS AND DATA REDUCTION TECHNIQUES

NOVEMBER 1970

prepared by
B. J. MATTHEWS and R. F. KEMP

CONTINUATION OF APCO CONTRACT CPA 70–4

NATIONAL TECHNICAL INFORMATION SERVICE

TRW SYSTEMS GROUP
ONE SPACE PARK • REDONDO BEACH • CALIFORNIA

75

BIBLIOGRAPHIC DATA SHEET	1. Report No. APTD-1065	2.	3. Recipient's Accession No.

4. Title and Subtitle
Investigation of Scattered Light Holography of Aerosols and Data Reduction Techniques

5. Report Date
November 1970

6.

7. Author(s)
B. J. Matthews and R. F. Kemp

8. Performing Organization Rept. No. 14103-6002-R0-00

9. Performing Organization Name and Address
TRW Systems Group
One Space Park
Redondo Beach, California

10. Project/Task/Work Unit No.

11. Contract/Grant No.
CPA 70-4

12. Sponsoring Organization Name and Address
ENVIRONMENTAL PROTECTION AGENCY
Office of Air Programs

13. Type of Report & Period Covered

14.

15. Supplementary Notes

16. Abstracts

Investigation was initiated to increase the utility of the holographic technique in its application to limestone plume distribution studies. The following results were achieved with respect to the program objectives: (1) the feasibility of holographically recording ruby laser backscatter from aerosols of flyash, chalk dust and incense; (2) a mathematical model was derived which yields particle number density estimates from forward low angle scattered light intensity measurements of reconstructed holographic images recorded under specified conditions; (3) pulsed ruby laser holograms of a dioctyl phthalate aerosol of known characteristics were recorded and used to verify the derived mathematical model; (4) a method of real image hologram reconstruction was demonstrated to facilitate direct measurement of scattered light intensities and corresponding spatial locations; (5) a computer program of the derived mathematical model was written and utilized for particle number data reduction. The smoke particles corresponding in size to the wavelength of ruby light were recorded. The report describes the apparatus and methods used in each of these major tasks.

17. Key Words and Document Analysis. 17a. Descriptors

Air pollution
Plumes
Plume detection
Limestone
Light scattering
Holography
Holograms
Ruby lasers
Mathematical models
Aerosols
Particles
Computer programs

17b. Identifiers/Open-Ended Terms

Particulates

17c. COSATI Field/Group 13B

18. Availability Statement	19. Security Class (This Report)	21. No. of Pages
Unlimited	UNCLASSIFIED	75
	20. Security Class (This Page) UNCLASSIFIED	22. Price

TRW REPORT NO. 14103-6002-R0-00

INVESTIGATION OF SCATTERED LIGHT HOLOGRAPHY OF AEROSOLS AND DATA REDUCTION TECHNIQUES

NOVEMBER 1970

prepared by
B. J. MATTHEWS and R. F. KEMP

CONTINUATION OF APCO CONTRACT CPA 70–4

Details of illustrations in this document may be better studied on microfiche

TRW
SYSTEMS GROUP
ONE SPACE PARK • REDONDO BEACH • CALIFORNIA

FOREWORD

This report summarizes theoretical and experimental work accomplished under the Air Pollution Control Office, Environmental Protection Agency Contract CPA 70-4, Modification No. 3, dated 31 July 1970. The report is submitted by TRW Systems Group, TRW Inc., in accordance with provisions of the modified contract.

Work on this contract was accomplished by personnel of the Science and Technology Division of TRW Systems Group. The Project Manager was Mr. B. J. Matthews. Dr. R. F. Wuerker served as Consulting Principal Scientist. Mr. R. F. Kemp was a participating Staff Engineer. Technical administration of the contract was initially the responsibility of Mr. Donald K. Felton of the APCO Division of Process Control Engineering. Midway through the program, the responsibility for technical direction was transferred to Dr. Fredric C. Jaye of EPA/APCO.

The authors are indebted to Drs. R. F. Wuerker and L. O. Heflinger for use of the TRW Chlorophyll dye cell ruby laser system which resulted in the first successful holography of laser backscatter over extended distances. Derivation of the mathematical model used in hologram data reduction was accomplished by Dr. R. S. Fraser of TRW's Research Staff. The work and cooperation of Messrs. R. A. Briones and D. E. Gallagher during the experimental test effort was a material aid to the success of the program.

Preceding page blank

CONTENTS

		Page
1.	INTRODUCTION	1-1
	1.1 Background Information	1-1
	1.2 Added Program Work	1-2
2.	RESULTS AND DISCUSSION	2-1
	2.1 Holography of Ruby Laser Backscatter	2-1
	2.2 Breadboard Holocamera Design	2-2
	2.3 Backscatter Holography Results	2-3
	2.4 Evaluation of Backscatter Holography Technique	2-6
	2.5 Preliminary Light Intensity Measurements	2-9
3.	SCATTERED LIGHT HOLOGRAM DATA REDUCTION	3-1
	3.1 Derivation of Equation	3-1
	3.2 Scattering Characteristics of Limestone - Flyash Mixtures	3-5
	3.3 Accuracy of Model	3-16
4.	LABORATORY VERIFICATION EXPERIMENTS	4-1
	4.1 Test Aerosol Selection and Generation	4-1
	4.2 Transmission Holocamera Apparatus	4-4
	4.3 Forward Scatter Holography and Reconstruction	4-7
	4.4 Hologram Data Reduction	4-10
	4.5 Experimental Results	4-13
5.	CONCLUSIONS	5-1
6.	RECOMMENDATIONS	6-1
	NOMENCLATURE	
	REFERENCES	
APPENDICES		
	A THE IMAGINARY PART OF THE INDEX OF REFRACTION	A-1
	B COMPUTER PROGRAM	B-1
	C AEROSOL DROPLET DENSITY	C-1

Preceding page blank

ILLUSTRATIONS

		Page
1.	Schematic diagram of holocamera used to record ruby laser backscatter	2-2
2.	Photograph of modified ruby laser	2-3
3.	Photomicrographs of chalk dust	2-5
4.	Typical reconstruction photo of chalk dust backscatter hologram	2-6
5.	Photomicrographs of incense smoke aerosol at LN_2 temperature	2-7
6.	Schematic of setup for preliminary scattering measurements	2-9
7.	Schematic representation of laser beam and receiving optics	3-2
8.	Photomicrographs of flayash sample from Unit 10 mechanical hoppers	3-7
9.	Additional photomicrographs of flyash from Unit 10 mechanical hoppers	3-8
10.	Photomicrographs of flyash from Unit 10 electrostatic precipitator hoppers 5-8	3-9
11.	Transmitted and reflected light (10X) photomicrographs of Unit 10 flyash from electrostatic precipitator hoppers 5-8	3-10
12.	Photomicrograph of flyash from Unit 10 electrostatic precipitator hoppers 1-4	3-11
13.	Electron microscope photograph (5340X) of flyash from Unit 10 electrostatic precipitator hoppers 1-4	3-12
14.	Electron microscope photograph (43, 350X) of flyash from Unit 10 electrostatic precipitator hoppers 1-4	3-13
15.	Scattering phase function $p/4\pi$	3-17
16.	Photomicrograph of pulverized Unit 10 limestone	4-2
17.	Photomicrograph of No. 60 mesh pulverized coal sample	4-2
18.	Photomicrograph of aluminum oxide powder	4-3

Preceding page blank

ILLUSTRATIONS (Continued)

		Page
19.	Photomicrograph of talcum powder	4-3
20.	Photomicrograph of styrene spheres	4-4
21.	Schematic diagram of scattered light three-beam transmission holocamera	4-5
22.	Schematic diagram of reconstruction apparatus	4-9
23.	Schematic diagram of reconstructed scene beam real image	4-12
24.	Particle density versus distance for hologram number 1781	4-14
25.	Particle density versus distance for hologram number 1782	4-14
26.	Particle density versus distance for hologram number 1783	4-15
27.	Particle density versus distance for hologram number 1784	4-15

LIST OF TABLES

		Page
I.	Backscatter Feasibility Demonstration Holograms	2-4
II.	Index of Refraction and Other Properties of Typical Gas Species and Entrained Solids in a Coal Fired Steam Boiler	3-14
III.	Liquids for Index by Immersion Methods	3-15
IV.	Efficiency Factors as a Function of α and of the Index of Refraction	3-16
V.	List of Candidate Aerosol Materials	4-1
VI.	Summary of Low Angle Forward Scattering Ruby Laser Transmission Holograms	4-8
VII.	Comparison of Calculated and Measured Values of n	4-17

1. INTRODUCTION

1.1 BACKGROUND INFORMATION

The penetration and dispersion of dry limestone clouds pneumatically injected into a 140-megawatt, 24-foot wide pulverized coal burning steam boiler has been successfully recorded using pulsed ruby laser transmission holography. Portions of the limestone plumes are visualized by holographically recording low angle forward scattered light caused by injected limestone particulate and flyash passing through the probing ruby laser beam. The development and demonstration of this two beam holographic instrumentation technique was previously accomplished during an 8-month, three-phase program sponsored by the Air Pollution Control Office of the Environmental Protection Agency. * The work culminated with a full-scale demonstration test at the Tennessee Valley Authority's Shawnee Power Plant in Paducah, Kentucky.

A two-beam pulsed ruby laser holocamera was installed on the Shawnee Unit 10 boiler and a series of scattered light holograms was recorded under a variety of boiler operating conditions. A complete description of the experimental apparatus, operating methods and results is presented in Reference 1 which is a final technical report issued at the conclusion of the basic APCO contract. In essence, the scattered light holographic technique was developed to the extent that detection and spatial resolution of injected limestone plumes was demonstrated. Plume penetration into the boiler was determined and the presence of plume structure or discrete voids identified and measured in the small volume of light visible through the observation ports.

Evaluation of the scattered light holograms recorded at the Shawnee Unit 10 boiler was accomplished with the aid of a ranging telescope calibrated for distance measurement. Viewing the reconstructed holographic virtual image, it was possible to focus on scattered light images of limestone clouds in the boiler. Further evaluation of the hologram virtual image was accomplished via photometric means. This was done by placing a view camera before the reconstructed holograms and photographing the scattered light image. The resulting negative was then used to make densitometry measurements of changes in image intensity.

The photometric data were used to make limestone cloud dimensional measurements (which correlated quite well with the telescopic observations) and to obtain information on the relative cloud intensities. Absolute limestone cloud intensity variations could not be obtained from the Unit 10 holograms since a suitable light intensity reference was lacking in the reconstructed images. For this reason, it was not possible to make direct comparisons between holograms nor to acquire quantitative data concerning the variation in limestone dust concentration as a function of hologram image intensity. The application of holography to the study of injected limestone plume formation and dispersion would be enhanced significantly, however, if local dust concentrations and time-phased

---

*APCO Contract No. CPA 70-4, dated 18 August 1969.

comparisons could be obtained directly from reconstructed scattered light images. For these reasons, additional program work was initiated following conclusion of the Shawnee Unit 10 holographic feasibility tests.*

1.2 ADDED PROGRAM WORK

The added scope work was designed specifically to increase the utility of the holographic technique in its application to limestone plume distribution studies. This feasibility work centered on the following objectives.

- Determine feasibility of holographing ruby laser back-scatter from aerosols.
- Derive a mathematical model of low angle forward scattered light from an aerosol of varying density over a large volume.
- Experimentally verify the scattered light mathematical model via controlled laboratory tests.
- Determine the practical size limitation of particles that may be detected by scattered light holographic techniques.

The feasibility of laser backscatter holography is important to the Shawnee Unit 10 limestone plume studies since the backscatter technique requires only one boiler port for equipment installation. In contrast, transmission holography requires the availability of two opposed ports in the boiler. Thus, some physical limitations with regard to equipment installation are minimized if a backscatter holographic technique can be utilized. The backscatter method is, however, not without inherent limitations. Advantages and limitations of each are discussed subsequently.

The formulation of a mathematical model to describe the low angle forward scattering of a transmitted ruby laser beam was utilized to estimate variations in aerosol particle number density in the reconstructed holographic scene. The third objective was to design and implement a controlled laboratory experiment to test the mathematical model prediction of the scattered light holographic image. The experimental work was successfully accomplished. The absolute limit of particulate size which can be detected via scattered light holography was not systematically investigated (the fourth objective); however, the dynamic range of the holographic method was rather dramatically demonstrated on a separate program.** In addition, the recording of smokes of micron and submicron size was demonstrated during the experimental portion of this program.

---

*Modification No. 2 to APCO Contract CPA 70-4, dated 16 June 1970.

**The work was sponsored by the National Aeronautics and Space Administration (NASA) under a contract to TRW Systems Group. The results of this work by Drs. L. O. Heflinger and R. E. Brooks is presented subsequently in the body of this report.

Subsequent sections of this report describe the apparatus and methods used in each of the major tasks. Results are presented and discussed in context with future applications of holography as an instrumentation technique for monitoring dry limestone plumes injected into the Unit 10 boiler.

2. RESULTS AND DISCUSSION

The added scope of work to APCO contract CPA 70-4 was initiated in June 1970. In the subsequent three month period, the following results were achieved with respect to the program objectives:

- The feasibility of holographically recording ruby laser backscatter from aerosols of flyash, chalk dust and incense over distances of up to 15 feet was demonstrated.
- A mathematical model was derived which yields particle number density estimates from forward, low angle scattered light intensity measurements of reconstructed holographic images recorded under specified conditions.
- Pulsed ruby laser holograms of a dioctyl phthalate (DOP) aerosol of known characteristics were recorded and used to verify the derived mathematical model.
- A method of real image hologram reconstruction was demonstrated to facilitate direct measurement of scattered light intensities and corresponding spatial locations.
- A computer program of the derived mathematical model was written and utilized for particle number data reduction.
- Limitations on particle size with respect to the scattered light holography technique was not fully explored; however, smoke particles corresponding in size to the wavelength of ruby light (0.69μ) were recorded.

2.1 HOLOGRAPHY OF RUBY LASER BACKSCATTER

At the time laser backscatter holography was proposed, it was acknowledged by TRW that this was a much more difficult task than holographically recording low angle forward scattering. The holography of laser back scatter (essentially reflected light holography) requires illuminators with extended temporal coherence. The pulsed ruby laser employed during the (Phase III) Shawnee holography work utilized an internal Kerr cell Q-switch.[1] It was known that this laser possessed limited coherence. It was planned to replace the electro-optical Q switch by a cryptocyanine dye cell. The dye cell acts to achieve longer ruby laser coherence[2].

In the interim period since the added scope work was begun, Drs. R. F. Wuerker and L. O. Heflinger of TRW's Physical Electronics Laboratory have demonstrated under a concurrent Air Force-sponsored program a new dye cell Q-switch (Chlorophyll d in a mineral oil base) which significantly extends the coherence length of a pulsed ruby laser.[3] One of the results of this development in laser technology was the recording of the first known low angle backscattered ruby light holograms over

distances up to 15 feet. * Even greater scene depth-of-field is feasible. Because the Chlorophyll d dye cell laser worked better than other dyes, no additional tests were made using cryptocynanine.

2.2 BREADBOARD HOLOCAMERA DESIGN

The "breadboard "reflected light holocamera used to demonstrate feasibility of "long distance" backscatter holography is shown schematically in Figure 1. ** The modified (Chlorophyll dye cell) TRW ruby laser and the general laboratory setup may be seen in the photograph of Figure 2. From the Figure 1 schematic, it will be seen that a reference beam is generated with a wedge beam splitter placed before the ruby laser output. A corner prism, diverging lens and front surface mirror are used to cast a (diverging) simple spherical wavefront reference beam onto the hologram. The unexpanded scene beam component is passed through the beam splitter and across the desired scene volume. Particulate in the scene beam path scatter the laser light in all directions. Backscatter components received by the film plate mix with the reference beam and form the interference pattern recorded by the plate. The developed plate becomes the hologram.

Reconstruction techniques and examination of the scattered light images is accomplished in a manner similar to that used with the forward scattering two-beam transmission holograms made during the previous APCO work. [4]

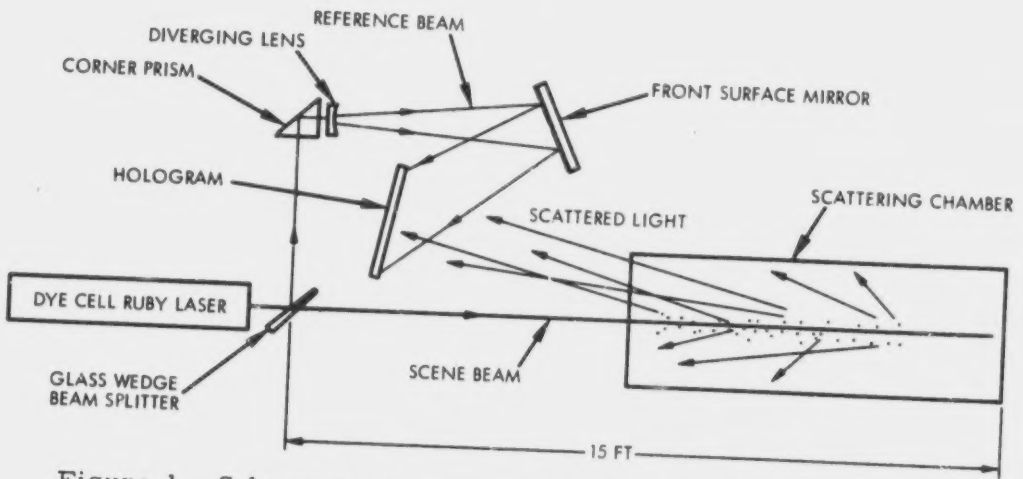

Figure 1. Schematic diagram of reflected light holocamera used to record ruby laser backscatter

---

*The 15-foot distance of the backscatter feasibility experiments was determined by physical space limitations imposed by the experimental laboratory.

**A similar test setup could be employed at the Unit 10 boiler. Specific boiler geometry conditions would impose some modification.

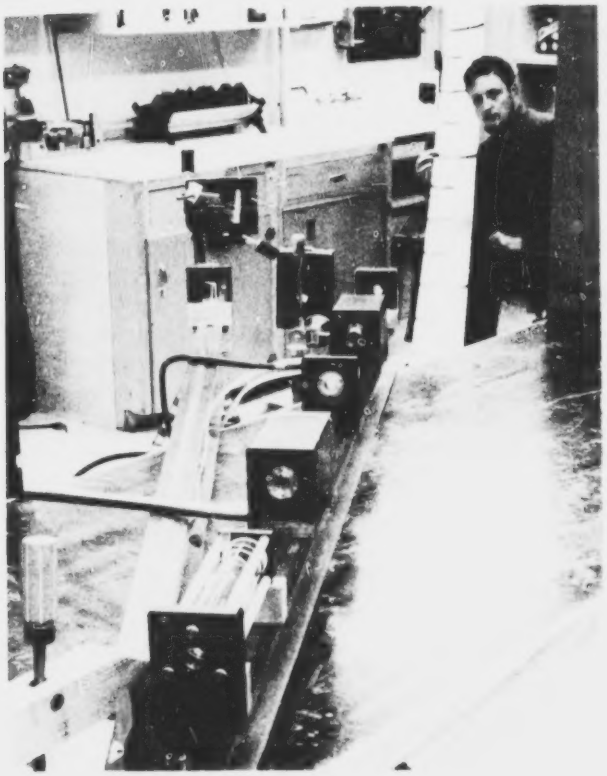

Figure 2

Photograph of the modified ruby laser and reflected light holocamera used to record laser backscatter. Film plate holder is just to left of laser rail. Reference beam mirror, corner prism, etc., are mounted on separate rail to left of laser. New laser dye cell is in the foreground of the photograph on the laser optical rail. The scattering chamber was placed in the scene volume occupied by long paper strip marked in 1/4 meter intervals.

2.3 BACKSCATTER HOLOGRAPHY RESULTS

Using the holocamera arrangement shown in Figure 1, a series of recordings was made using both a liquid aerosol (religious incense) and chalk dust. *

Backscatter holograms were also made in an open room with a maximum scene beam optical path of 15 feet. Only chalk dust was used for these recordings.

Additional recordings were made with the aerosols confined in a "scattering chamber" 18 x 18 x 74 inches in dimension. The chamber had acrylic windows on each end and along the 74-inch length of one side. The latter was for visual observation of the generated aerosol. The probing laser beam traversed the 74-inch length of the chamber.

Provisions were made for inserting two acrylic panels to partition the chamber into three separate volumes (each approximately two feet in length) such that an aerosol could be separately generated in one or more volumes. In this manner, an aerosol cloud with an artificial void could

*The liquid aerosol was produced by burning an abbatial blend of Trappist Monk Incense obtained from the Abbey of Our Lady of New Melleray, Dubuque, Iowa. Chalk dust was created by simply tapping two blackboard erasers together along the path of the laser beam.

be holographically recorded, reconstructed, and the image measured for spatial location and detail. The partitioned scattering chamber results were only moderately successful, since the extraneous reflections from the surfaces of the acrylic partitions yielded confusing sets of images in the reconstructed holograms.

A list of holograms recorded during the feasibility demonstration of backscatter holography is shown in Table I. A variety of test conditions were recorded using both incense and eraser chalk dust. The chalk dust was examined visually using a microscope* and found to vary over a wide size range from a few microns to over 100 microns. Photomicrographs of chalk dust at magnifications of 10x and 60x were made using polaroid Type 42 ASA 200 film. Examples of these photomicrographs are shown in Figure 3.

Table I. Backscatter Feasibility Demonstration Holograms

Date	Record No.	Test Scene	Remarks
7-24-70	3	Chalk dust	Good hologram
	4	Chalk dust	Short second laser pulse
	B-1	Chalk dust	Laser double pulsed
	B-2	Chalk dust	Laser double pulsed
	B-3	Incense	Scattering chamber, good hologram
	B-4	Incense	Good hologram, same as B-3
	B-5	Incense	Laser double pulsed
	B-6	Incense	No recording, shutter not opened
	B-7	Incense	Laser double pulsed
	B-8	Incense	Scattering chamber, good hologram
	B-9	Incense	Partitions in chamber, center section empty, smoke in both outer volumes.
	B-10	Incense	Same as B-9 but laser double pulsed
	B-11	Incense	Same as B-9
	B-12	Incense/Chalk	Outer two volumes of chamber filled with smoke, center section with chalk dust
	A	Chalk dust	No chamber used, 15 ft scene beam across laboratory, good hologram
	B	Chalk dust	Same as A
	C	Chalk dust	Same as A
	D	Chalk dust	Same as A

*Izumi Polarization Microscope, serial number 19637.

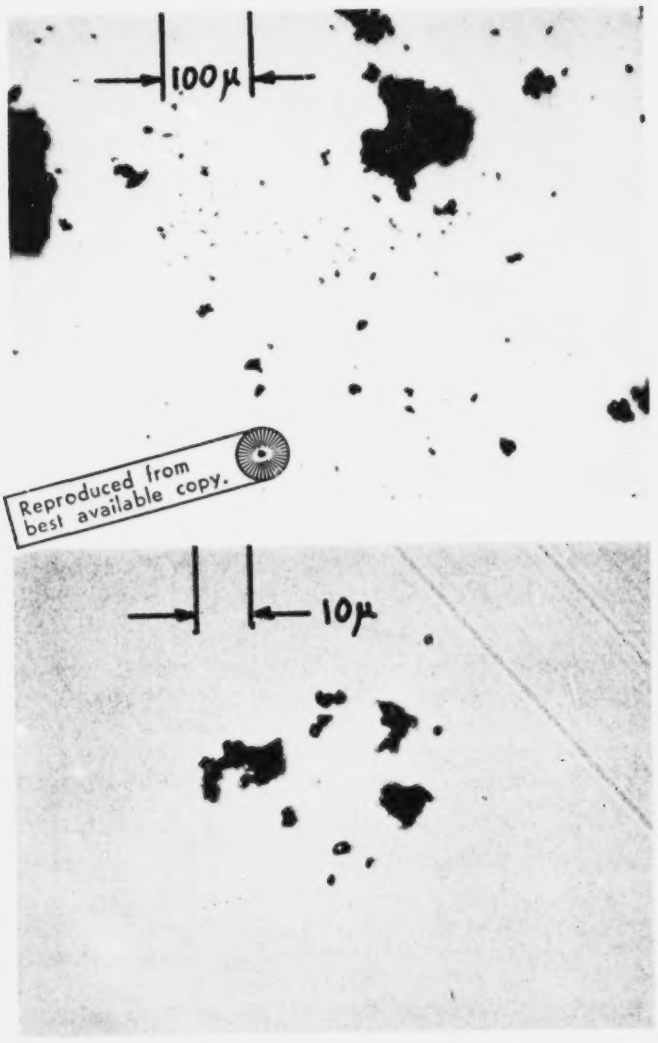

Figure 3. Photomicrographs of chalk dust from blackboard erasers. Magnification is 10X and 60X of upper and lower photos, respectively.

A reconstruction photograph of a chalk dust backscatter hologram is shown in Figure 4. The wide size range of these dust particles produced dramatic reconstructions. It was possible to focus on discrete scattered light images. By varying one's position with respect to the hologram reconstruction, the backscatter intensity distribution as a function of angle could be observed for a given scattered light image. In theory, one could deduce estimates of particle size by measuring the radiation patterns of discrete particles in an ensemble. The feasibility of this type of measurement for forward scattering by water droplets was demonstrated by Hickling at the General Motors Corp. Research Laboratories. [5]

Figure 4. Typical reconstruction photograph of chalk dust particles distributed over a distance of about 15 feet. The presence of the particles is detected by the low angle backscatter of the probing ruby laser beam.

The backscatter holograms of incense smoke were not as dramatic in appearance as the chalk dust recordings; however, the incense provided a more convenient aerosol from the standpoint of generation and control. * The incense smoke tended to rapidly diffuse throughout the scattering chamber and had excellent lingering qualities. It also produced predominantly small particle sizes. Microscopic examination confirmed that this smoke consisted primarily of micron-sized particles. Since this aerosol is either liquid or like wax, direct optical measurement of individual droplets is difficult. In the end, microscope slides were immersed in liquid nitrogen (LN_2) and subsequently passed through the aerosol. ** Condensed aerosol droplets were then examined under a measuring microscope. Photomicrographs of incense droplets sampled in this manner are illustrated in the photographs of Figure 5. The larger droplets are probably the result of coalescence during the sampling process.

2.4 EVALUATION OF BACKSCATTER HOLOGRAPHY TECHNIQUE

Ultimately, the applicability of backscatter holography to the detection of limestone plumes in Unit 10 is dependent upon the scene depth-of-field which can be obtained with respect to plume geometry and physical location using a given boiler port. The original limitation of

---

*Later in the test program, another liquid aerosol of known properties (dioctyl phthalate: DOP) was used because the refractive index of incense could not be readily obtained from the literature.

**LN_2 boiling point is -320°F at one atmosphere.

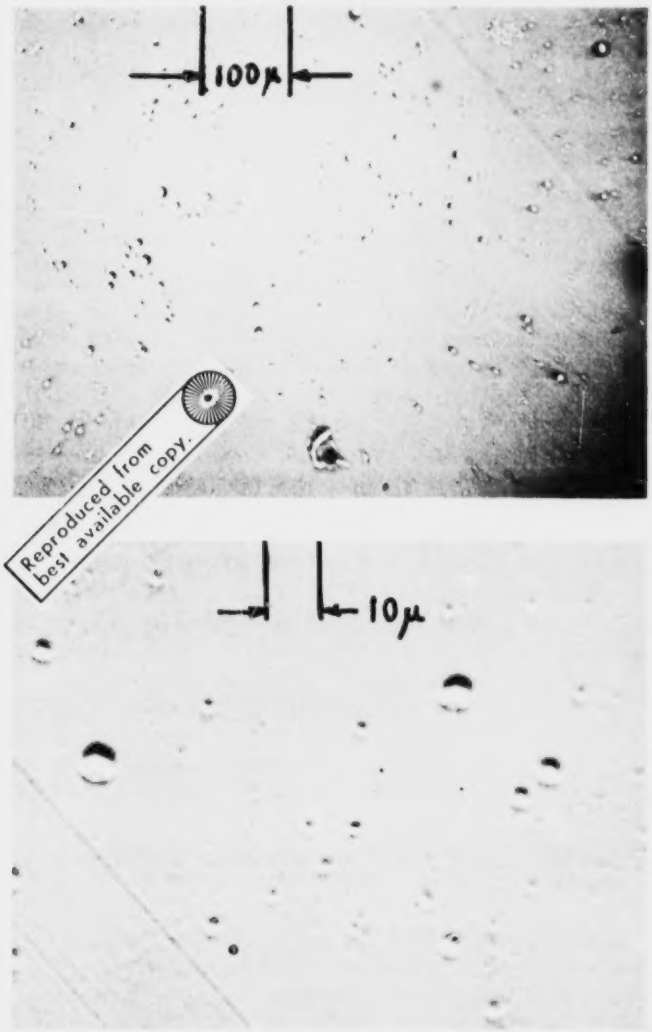

Reproduced from best available copy.

Figure 5. Photomicrographs of incense smoke liquid aerosol at LN_2 temperature. Magnifications are 10X and 60X for upper and lower photos, respectively.

laser coherence was overcome with the development of the Chlorophyll d dye cell Q-switch. Limitations on the backscatter technique now center on questions concerning the attenuation of laser light by the scattering medium, beam divergence (energy per unit area) and the available total energy which can be generated by the ruby illuminator. Of these three considerations, scene light attenuation is by far the most significant. Beam divergence is comparatively small. The amount of coherent laser energy is limited to 2-3 joules for a moderate sized ruby laser illuminator.

In backscatter holography, the probing laser beam is attenuated to an intensity I after transmission through the scattering media a distance x by the relationship

$$I = I_o e^{-\mu x}$$

where I_o is the incident laser beam intensity, e is the base of the natural system of logarithms (2.718. . . .) and μ is an optical attenuation coefficient per unit length. The attenuation coefficient is equal to the product $n\sigma$, where n is the number density of particles in the beam path and σ is the extinction cross-section per particle. That portion of the backscattered laser light received by the hologram is further attenuated by the same relationship in traveling back over the distance x. Consequently, the distance x in the exponent is increased by a factor of two. Further, there is a $1/x^2$ dependence of the scattered radiation with respect to the hologram since the scattered light is not collimated but rather throws the light over a large solid angle. Therefore, only a small portion of the radiant energy from the scatterer is incident back onto the hologram. A simplified expression then, for the intensity of the returned scattered laser signal is:

$$I \propto \frac{I_o e^{-\mu 2x}}{x^2}$$

The impact of increasing the distance x on the intensity of the backscattered light received by the hologram is evident.

Compensating at least in part for the weak return signal one may expect from backscatter holograms of heavily attenuated scenes is the sensitivity of the holographic technique. The transmission holography tests described subsequently (Section 4.2) utilized what may be called a "three-beam" holocamera arrangement. In essence, the reference beam is divided into two components and then recombined together with the scene beam at the plane of the hologram. This configuration has the feature that a hologram is always recorded regardless of the intensity of the scene beam. An interference pattern always occurs between the wavefronts of the two reference beams. In the absence of any scene beam signal, the hologram behaves as a simple diffraction grating. The presence of a scene beam signal modulates the basic diffraction grating and allows reconstruction and observation of the scene image. It has been demonstrated that a single point source scene beam may be attenuated to a factor of 10^{-6} less than the reference illumination and still be observed in the hologram reconstruction.[6]

The extreme sensitivity of the holographic technique using a three-beam configuration suggests that backscatter holography of Unit 10 limestone and flyash ensembles is feasible. The extent that the probing ruby laser beam will penetrate into the boiler remains to be determined. The recent laboratory tests demonstrated that reconstructions of laser

backscatter from dense aerosols (incense smoke) over distances of 6 feet could be accomplished. These tests, using the scattering chamber, were made with values of the optical attenuation coefficient/unit length $\mu \cong 0.14$ ft^{-1} which is very close to preliminary values of μ measured at both the TVA Galatin and Shawnee steam plants.[7]

2.5 PRELIMINARY LIGHT INTENSITY MEASUREMENTS

Preliminary light intensity measurements as a function of viewing angle (0 to 180°) were made early in the added scope work. The purpose of such tests was to obtain qualitative and quantitative information to assess the feasibility of backscatter holography, and utilize these measurements as an aid to interpreting (possible) future holograms made to the Unit 10 boiler.

Accordingly, measurements were made using dilute suspensions of soap and also of tea in a glass beaker of water as shown in the schematic of Figure 6. Difficulties in scaling the experiment to represent light attenuation levels equivalent to (nominal) Unit 10 conditions were encountered. Not only must the suspension attenuate the probing beam relative to the boiler gas flow, but the geometric relationship of the transmitting and receiving optics (at any given angle) must also scale since the intensity of the returning or scattered light is inversely proportional to the square of the distance r involved.

It was also found that the internal glass (beaker) surfaces reflected light of the probing helium neon gas laser beam introducing further measurement error. (The cylindrical beaker was originally selected for reasons of experimental simplicity.)

In the interim, a pulsed ruby laser possessing excellent temporal coherence was developed (Section 2.2) which immediately made the

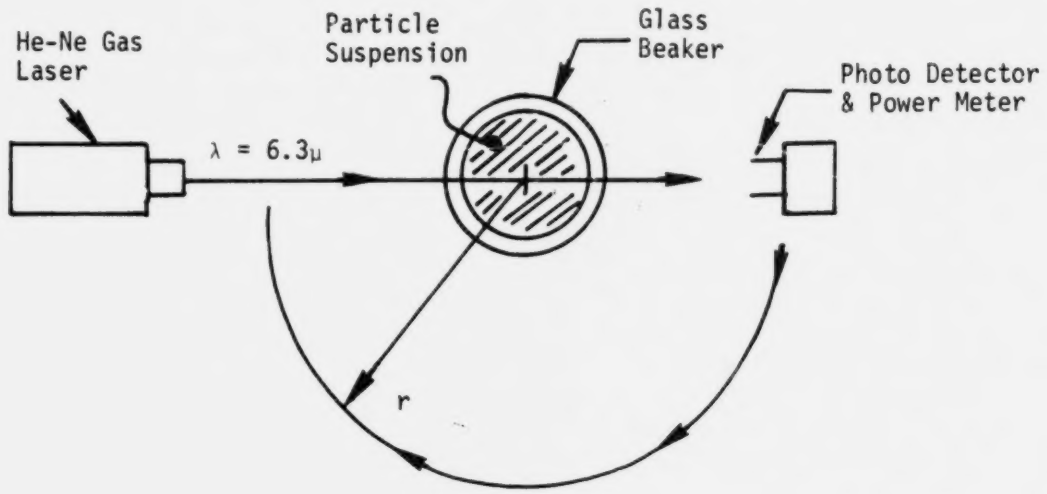

Figure 6. Schematic of setup for preliminary scattering measurements

recording of laser backscatter a practical matter. In brief, the value of preliminary light scattering measurements was no longer important to the development of a backscatter holography capability. No additional work was done on scattering with a helium-neon continuous wave gas laser.

3. SCATTERED LIGHT HOLOGRAM DATA REDUCTION

A mathematical model has been derived which predicts the intensity of light scattered in the forward direction of an optical detector from an aerosol of varying density over a large volume. The equations can be solved for the number density of aerosol particles from the brightness variations in a holographically recorded image of low angle forward scattered light. Certain assumptions are required concerning the scattering properties of the various aerosol species; these are discussed. Formulation of the basic mathematical model was done by Dr. R. S. Fraser of TRW Systems Group Research Staff.

3.1 DERIVATION OF EQUATION

Holograms of low angle forward scattering have been made by transmitting a pulse of ruby laser light through an aerosol. Light is scattered in all directions by particles in the path of the laser beam. Components of the light scattered at low angles in the forward direction are received by the hologram. The scattered light interferes with a reference beam (passed around the scene) at the plane of the hologram. The result is a three-dimensional image of the intensity distribution of scattered light "frozen" in an instant of time.*

To interrogate the reconstructed scattered light image, equations relating the scattered power and the density of the particles are required. Further, the geometric coordinates and variables must be defined. The schematic of Figure 7 represents the general case of a laser beam passing through an aerosol and an optical detector (hologram) positioned to receive a portion of the forward scatter. The centerline of the laser beam is concident with the x-axis, and its origin is at the left-hand boundary of the scattering volume. The point Q represents the intersection of the axes of the laser beam and of the optical detector. The right boundary of the scattering volume and the detector are both taken as x = L. The vertical distance of the detector from the x-axis is z. The distance from the detector to the point Q is y, given by

$$y = (\cos\theta)^{-1}(L - x)$$

$$\doteq (L - x)\left[1 + \frac{1}{2}\left(\frac{z}{L - x}\right)^2\right], \qquad z \ll L - x, \tag{1}$$

*The ruby laser pulse duration is ~50 nanoseconds or 50×10^{-9} seconds. Particle movement during the laser pulse is essentially negligible at the relatively low gas velocities in the furnace. For example, assume a particle moves at a velocity of 50 ft/sec or 600 in./sec. During a 50×10^{-9} sec laser pulse, the particle movement will be $600 \times 50 \times 10^{-9} = 0.00003$ inch or 0.75μ. At 100 ft/sec, particle movement is 1.5μ, etc.

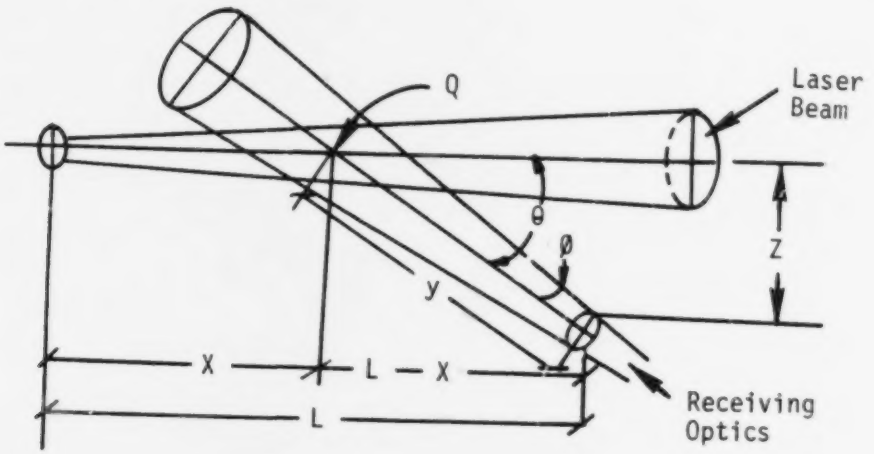

Figure 7. Schematic Representation of Laser Beam and the Cone for the Receiving Optics

where θ is the angle between the directions of the incident beam and scattered laser energy entering the detector.

The power (P) which is incident on a small area (ΔA) of the receiver objective is given by the following expression:

$$P(x) = P(0)T(x)n(x)\Delta V(x)\frac{\sigma_\ell}{\Sigma(x)}\frac{p(\theta(x))}{4\pi}T(y(x))\frac{\Delta A}{[y(x)]^2} \qquad (2)$$

P(0) is the laser power incident at the edge of the aerosol where x = 0.
T(x) is the transmission factor from the edge of the aerosol to the point x.
T(y) is the transmission factor from the point Q to the receiver objective. The expression for the transmission is of the form:

$$T(x) = \exp(-n\sigma_e x), \qquad (3)$$

where σ_e is the average extinction cross-section per particle. ΔV is the volume of the intersection of the laser beam with the receiving cone. n is the number density of particles; nΔV gives the number of particles in ΔV. σ is the average scattering cross section of a single particle. The term $[(4\pi)^{-1}\, p(\theta(x))]$ is the scattering phase function. It has the following property:

$$\frac{1}{4\pi}\int_0^{2\pi}\int_0^{\pi} p(\theta)\sin\theta\ d\theta\ d\phi' = 1, \qquad (4)$$

where θ has already been defined and ϕ' is an azimuthal coordinate. The area of the laser beam cross-section that is normal to the x-axis is:

$$\Sigma(x) = \pi r^2 = \pi(r_o + \beta x)^2 \tag{5}$$

where r_o and r equal the radii of the laser beam at $x = 0$ and at x, respectively; and $\beta = dr/dx$. The area of the receiver cone cross section (γ) that is normal to the receiver axis is given by:

$$\gamma(x) = \pi(\phi y(x))^2 \tag{6}$$

where ϕ is the half-angle of the receiver cone.

The volume ΔV will be related to the area of a laser beam image that is scanned by a densitometer or optical detector. It will be assumed here that the densitometer scans a small circular area that is centered on the center line of the image of the laser beam. The area scanned by the densitometer will determine ϕ of Equation (6), and ϕ will then be a constant independent of x. Since the volume ΔV is small, the laser beam and the receiver cone are assumed to be right circular cylinders locally in the vicinity of the point Q. Then the approximate volume of the intersection is:

$$\Delta V(x) \approx 2\pi\phi^2(L - x)^3(r_o + \beta x)z^{-1}. \tag{7}$$

When Equations (5) and (7) for the area and volume and Equation (1) are substituted in Equation (2), the equation for the ratio of the scattered to incident power becomes:

$$\frac{P(x)}{P(0)} = \frac{2n(x)\phi^2(L - x)\sigma_\ell T(L)}{z(r_o + \beta x)} \frac{p(\theta(x))}{4\pi} \Delta A. \tag{8}$$

Although the particle density n(x) can be computed from Equation (8), another procedure will be suggested.

The particle number density at a point will be expressed as the sum of the densities of the particles that are present as background (n_b) (e. g., flyash), the average density of injected particles ($\bar{n}$) (limestone dust), and the deviation of the density of injected particles from the average (ϵ):

$$n(x) = n_b + \bar{n} + \epsilon(x). \tag{9}$$

The density of the background particles is assumed to remain approximately the same before and during the experiment. The average of the deviation density for the propagation path is zero

$$\bar{\epsilon} = L^{-1} \int_o^L \epsilon(x)\, dx = 0. \tag{10}$$

The scattering cross-section per unit volume ($\sigma_\ell n$), which appears in Equation (8), can now be expressed in terms of the densities given by Equation (9):

$$\sigma_\ell n = (\bar{n} + \epsilon)\,\sigma + n_b \sigma_b, \tag{11}$$

where σ and σ_b are the average scattering cross-sections of an injected particle and of a background particle, respectively.

In order to measure the particle densities, two transmission measurements are required in addition to the hologram. The background density of particles (n_b) that are present before additional particles are injected into the combustion gas can be obtained from a transmission measurement before the hologram is made. In this case the transmission through a distance L of the aerosol is:

$$T_1(L) = P_1(L)/P(0) = \exp(-n_b \sigma_b L), \tag{12}$$

or the density of background particles is:

$$n_b = -\frac{1}{\sigma_b L}\, \ell n[P(L)/P(0)]. \tag{13}$$

where σ_b is the average extinction cross-section of the background particles.

The average density of injected particles can be obtained by measuring the transmitted power in the laser beam during an experiment. The transmission through the aerosol of thickness L is:

$$T_2(L) = \frac{P_2(L)}{P(0)} = \exp\left[-(n_b \sigma_b + \bar{n}\sigma)L\right]$$

$$= \frac{P_1(L)}{P(0)} \exp(-\bar{n}\sigma L) \tag{14}$$

It is assumed that the background density n_b is not changed by the experiment. Also, in both Equations (12) and (14), the combustion gases are assumed to have a negligible effect on the transmission. The average number density of injected particles can be obtained from Equations (12) and (14):

$$\bar{n} = \frac{1}{\sigma L} \ell n\left[P_2(L)/P(0)\right] - \frac{\sigma_b n_b}{\sigma} = \frac{1}{\sigma L} \ell n(P_2(L)/P_1(L)) \qquad (15)$$

The powers P(0) and P(L) are measured. n_b is measured by a different transmission experiment. The extinction cross-sections σ and σ_b are assumed known.

The deviation in the density of the injected particles is obtained by substituting Equation (11) in Equation (8):

$$\epsilon(x) = \frac{1}{\sigma}\left[\frac{P(x)}{P(0)} \frac{1}{2\phi^2} \frac{z}{(L - x)} (r_o + \beta x)\right.$$

$$\left. \cdot \frac{4\pi}{p(\theta(x))} \frac{1}{T(L)} \frac{1}{\Delta A} - (\sigma \bar{n} + \sigma_b n_b)\right]. \qquad (16)$$

In Equation (16) the measured quantities are the ratio of the power scattered in the direction of the receiver (P(x)) to the incident power (P(0)) and the transmission which is measured during an experiment. The scattering parameters ($p/4\pi$, σ, σ_b) in Equation (16) are assumed to be known. The number densities $\bar{n}$ and n_b are obtained from transmission measurements. The remaining parameters in Equation (16) are geometrical measures.

3.2 SCATTERING CHARACTERISTICS OF LIMESTONE - FLYASH MIXTURES

In order to estimate the accuracy with which Equation (16) can be used to compute the density deviation (ϵ), the scattering parameters have to be known. In applying the mathematical model to conditions in the Shawnee Unit 10 boiler, it is necessary to consider both the background particles (flyash) and the injected limestone particles ($CaCO_3$). A knowledge of the particulate characteristics is essential.

Scattering characteristics for a single particle depend upon its shape, size and index of refraction. Some information on particle size and shape is available. Flyash (only) samples taken from the Unit 10 electrostatic precipitator inlet indicate that 80 to 90 percent of the particles are less than about 30 microns and about 2 to 8 percent are reported to be smaller than 3.2 micron.[8] Limestone - flyash mixtures sampled at Plane C-C and Plane A-A in Unit 10 during Test P-2 on 29 January 1970, produced similar results.[9] In these samples, 60 to

80 percent of the particulate was less than about 30 microns in size. Only 3 percent were less than 3 microns in size. If one assumes a mean diameter of 3 microns, such particles are still large compared to the wave length of ruby light which is 0.69 micron. As a result, the scattering parameters used in Equation (16) of Section 3.1 are not sensitive to shape.[10, 11]

It is interesting to note that limestone-flyash samples collected from both the Unit 10 mechanical hoppers and electrostatic precipitator hoppers are predominately spherical and exhibit a transparent appearance. This may be seen in the photomicrographs of Figures 8 through 12. The spherical nature of the limestone-flyash particles is more dramatically illustrated in the electron microscope photographs of Figures 13 and 14*.

The indices of refraction for flyash compositions are not precisely known at this time. The composition will vary depending on the type of coal and conditions of combustion. Basically, the ash is a fused siliceous residue in the shape of glassy spheres.[12] The four primary constituents are: silicon dioxide (SiO_2); aluminum oxide (Al_2O_3); ferric oxide (Fe_2O_3); and calcium monoxide (CaO). Other minor constituents include magnesium oxide (MgO) and sodium monoxide plus potassium monoxide ($Na_2O + K_2O$). In the absence of injected limestone, the flyash constituents will typically vary over the following ranges:[13]

Constituent	Percent Range
SiO_2	40 to 60
Al_2O_3	20 to 60
Fe_2O_3	5 to 25
CaO	1 to 15
MgO	0.5 to 4
$Na_2O + K_2O$	1 to 4

The preceding discussion is related to coal combustion in the absence of any limestone ($CaCO_3$) injection into the boiler. The effect of limestone addition to the Shawnee Unit 10 was recently reported by J. S. Morris of the Tennessee Valley Authority.[14] At a 1.7 stoichiometric limestone injection operating condition, the amount of CaO in the limestone-flyash mixture was approximately 41 percent. Simultaneously, solids entrained in the combustion gas stream increased more than 80 percent. In summary, the index of refraction will be affected by the

---

*The micrographs of Figures 13 and 14 were made courtesy of C. Marinoff of TRW Systems Group using an Associated Electrical Industries of England, Model EM-6 electron microscope.

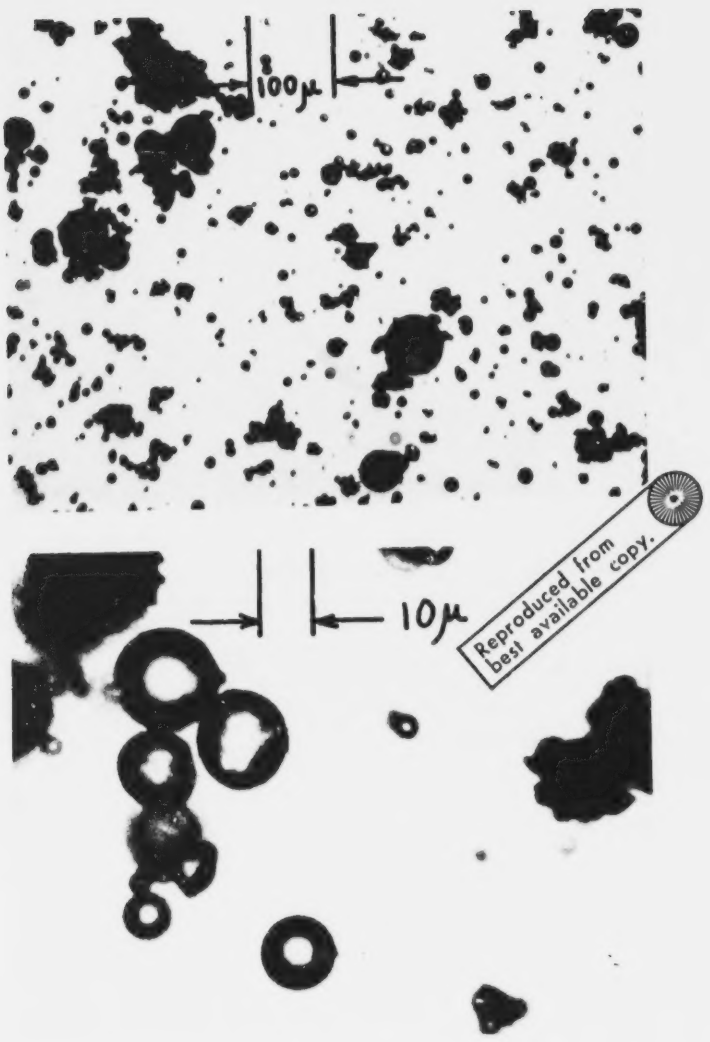

Figure 8. Photomicrographs of flyash sample collected from Unit 10 mechanical hoppers (No. 's. 1-8) while limestone was being injected into boiler. Magnification is 10X and 60X for upper and lower photos, respectively. (Refer to NAPCA/TVA limestone injection test P-2, 29 January 1970).

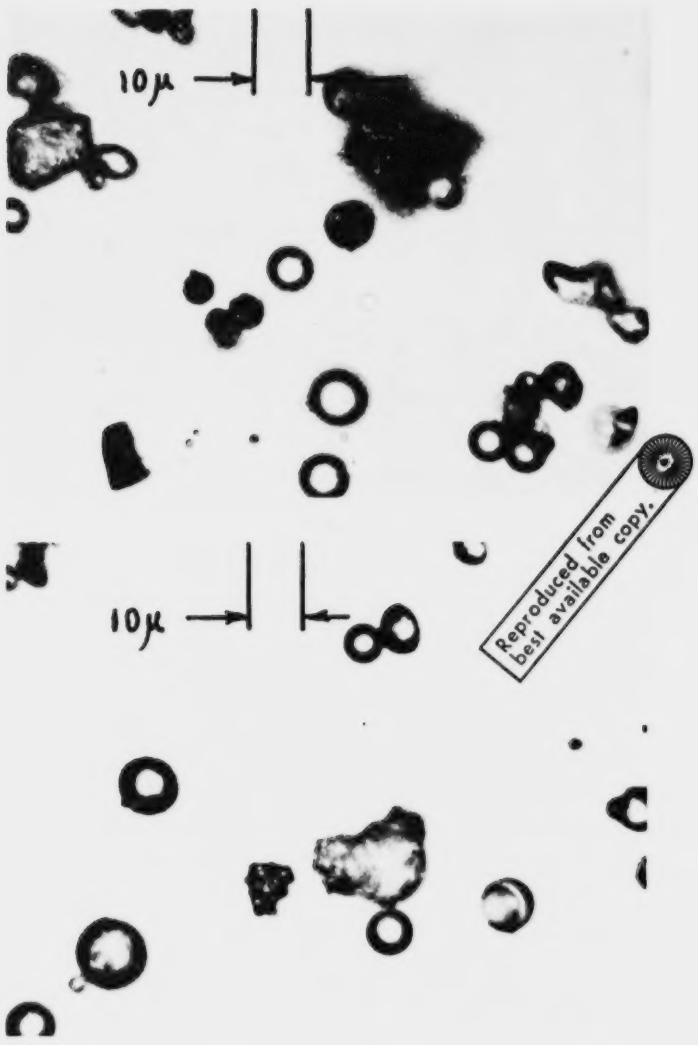

Figure 9. Additional 60X photomicrographs of flyash (with limestone) collected from the Unit 10 mechanical hoppers. Photos correspond to 60X enlargement in preceding figure. (Test P-2 on 29 January 1970.)

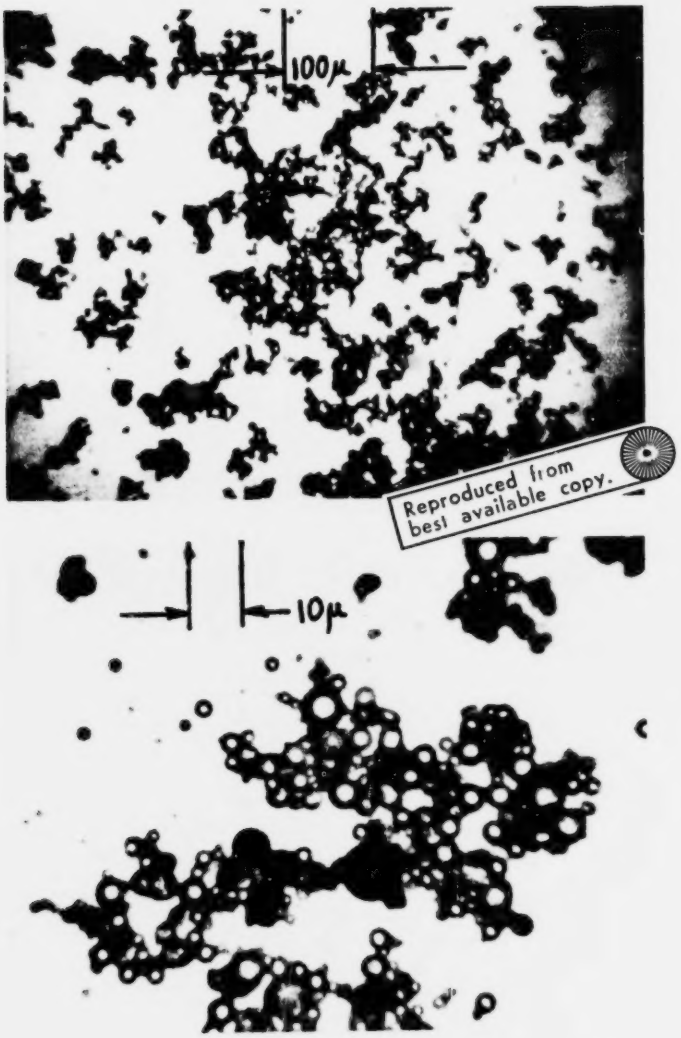

Figure 10. Photomicrographs of flyash sample collected from Unit 10 electrostatic precipitator hoppers numbers 5 through 8 (inlet side) while limestone was being injected into boiler. Magnification is 10X and 60X for upper and lower photos, respectively.

Figure 11. Transmitted and reflected light (10X) photomicrographs of Unit 10 flyash. Sample flyash collected from electrostatic precipitator hopper numbers 5 through 8 while limestone was being injected into Unit 10 boiler.

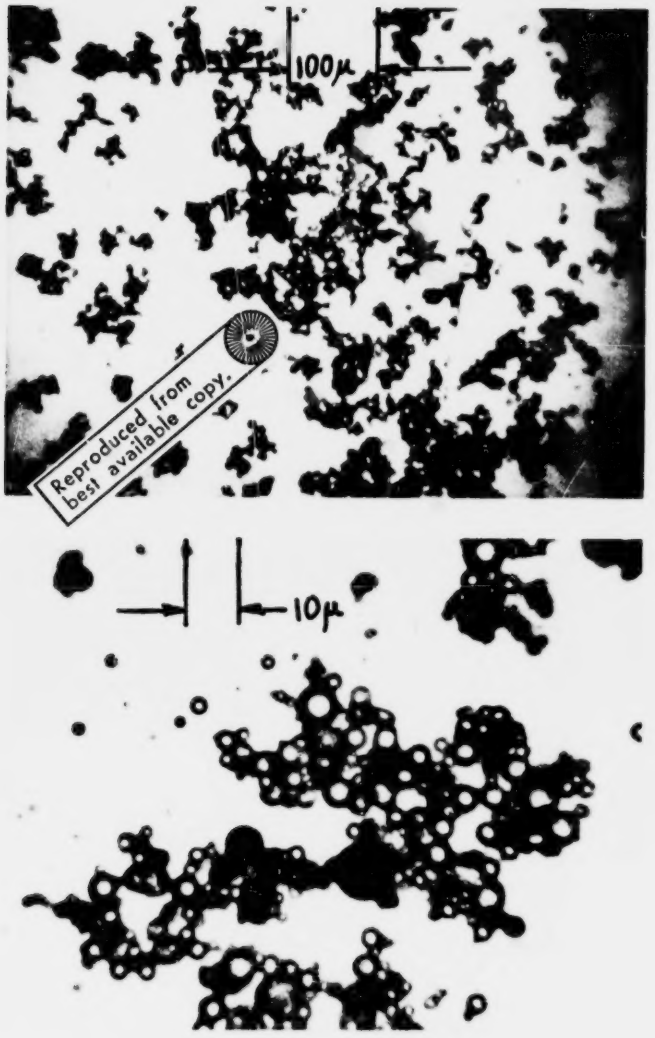

Figure 10. Photomicrographs of flyash sample collected from Unit 10 electrostatic precipitator hoppers numbers 5 through 8 (inlet side) while limestone was being injected into boiler. Magnification is 10X and 60X for upper and lower photos, respectively.

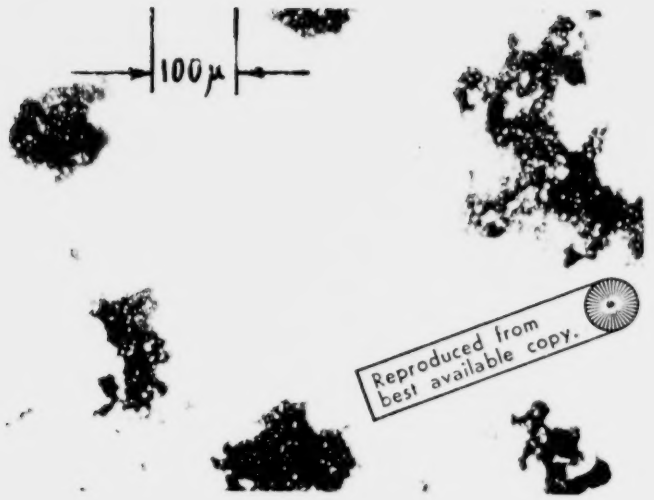

Reproduced from
best available copy.

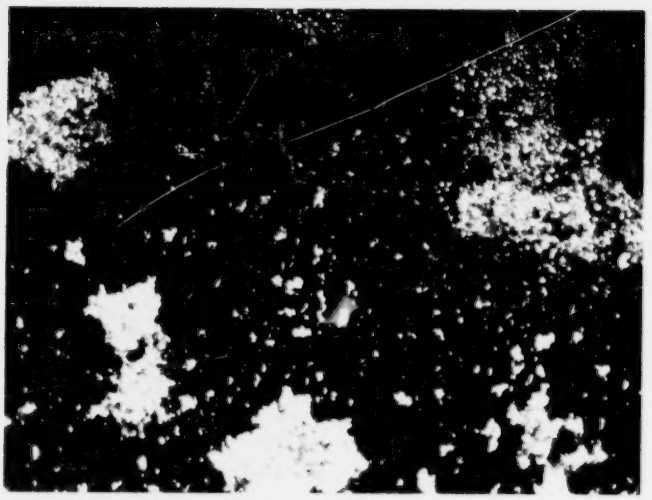

Figure 11. Transmitted and reflected light (10X) photomicrographs of Unit 10 flyash. Sample flyash collected from electrostatic precipitator hopper numbers 5 through 8 while limestone was being injected into Unit 10 boiler.

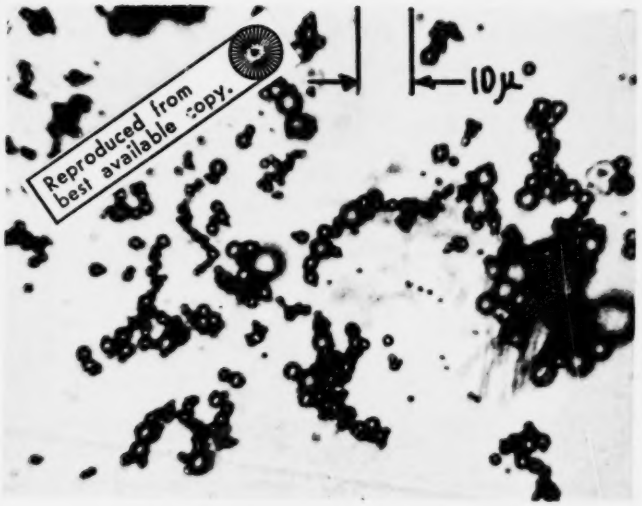

Figure 12

Photomicrograph of flyash sample collected from Unit 10 electrostatic precipitator hopper numbers 1 through 4 (outlet side) while limestone was being injected into boiler. Compare this transmitted light photomicrograph with subsequent two electron microscope photographs of Figures 13 and 14.

composition of Unit 10 limestone-flyash mixtures. The degree of change in the refractive index should be assessed. The index may have an imaginary part and particle scattering has a significant dependence on the imaginary index of refraction.*

A preliminary review of the properties of various solid and gaseous constituents in the Unit 10 gas stream are presented in Table II. A composite index or range of index values will ultimately have to be determined. One practical method described by W. C. McCrone is the immersion of a particulate sample into a medium of known refractive index.[15] Table III is a list of liquids possessing a range of indices which can be used as standard mediums.[16]

The particle extinction cross-section σ_e is the sum of the absorption (σ_a) and scattering (σ_s) cross-sections:

$$\sigma_e = \sigma_s + \sigma_a \tag{17}$$

Corresponding to these three cross-sections are three efficiency factors which equal the cross-section divided by the geometric cross-sectional area. If the particulates are spheres of radius a, the efficiency factors are:

$$Q_e = \sigma_e/\pi a^2 \quad ; \quad Q_a = \sigma_a/\pi a^2 \quad ; \quad Q_s = \sigma_s/\pi a^2 \tag{18}$$

---

*See Appendix A for a brief discussion on the imaginary part of the index of refraction.

Figure 13. Electron microscope photograph of flyash sample collected from Unit 10 electrostatic precipitator hoppers 1 through 4 (outlet side) while limestone was being injected into boiler. Magnification is 5340X.

Figure 14. Electron micrograph of flyash-limestone sample from Unit 10 electrostatic precipitator hoppers 1 through 4. Magnification is 43, 350X.

Table III Liquids for Index by Immersion Method

Liquid	Index at 100.8°F (24°C)
Trimethylene chloride	1.446
Cineole	1.456
Hexahydrophenol	1.466
Decahydronaphthalene	1.477
Isoamylphthalate	1.486
Tetrachloroethane	1.492
Pentachloroethane	1.501
Trimethylene bromide	1.513
Chlorobenzene	1.523
Ethylene bromide + Chlorobenzene	1.533
o-Nitrotoluene	1.544
Xylidine	1.557
o-Toluidine	1.570
Aniline	1.584
Bromoform	1.595
Iodobenzene + Bromobenzene	1.603
Iodobenzene + Bromobenzene	1.613
Quinoline	1.622
α-Chloronaphthalene	1.633
α-Bromonaphthalene + α-Chloronaphthalene	1.640-1.650
α-Bromonaphthalene + α-Iodonaphthalene	1.660-1.690
Methylene iodide + Iodobenzene	1.700-1.730
Methylene iodide	1.738
Methylene iodide saturated with sulfur	1.78
Yellow phosphorus, sulfur and methylene iodide*	2.06

*In a weight ratio of 8:1:1. Can be diluted with methylene iodide to cover range 1.74-2.06. For precautions in use, cf. West. Am. Mineral, 21 p. 245-9 (1936).

(Table IV) was selected and corresponding values of Q_e and Q_s were calculated as being representative.

The phase functions that are computed for spheres are given in Figure 15. The forward scattering angle varies approximately between 0 and 3 degrees during the laboratory and Shawnee experiments.* The curves are labeled with α on the left and diameter on the right. The given diameters apply when the wavelength $\lambda = 0.6328\mu$. As the particle diameter increases from 1μ to 4μ, the phase function increases monotonically. The phase function becomes more complicated for larger spheres because the diffraction minimum appears. If the sphere diameter is 3μ, the phase function decreases by 25 percent as the scattering angle increases from 0 to 3 degrees. The computed phase functions are insensitive to changes

*This assumes that the same Unit 10 port geometric configuration is maintained (refer to Reference 1, in particular, see pages 20-21).

Table IV. Efficiency Factors Q_e and Q_s as a Function of α and the Index of Refraction

	Index of Refraction						
α	1.68	1.68 - 0.1i		1.48	1.8 - 0.09i		2.0 - 0.4i	
	Q_e	Q_e	Q_s	Q_e	Q_e	Q_s	Q_e	Q_s
5	2.03							
10	1.94							
15	1.91	2.30	1.18	1.98	2.33	1.24	2.31	1.26
20	1.98							
40	2.23							
80	2.05							
160	2.08							
320	2.03							

Notes: 1) The term i in the index of refraction refers to imaginary part, i.e.; $i = \sqrt{-1}$.

2) $\alpha = 2\pi a/\lambda$.

in the index of refraction for the angular region between the directions of the incident laser beam and the first diffraction minimum. Experimental data also show that the phase function is insensitive to the shapes of particles for the angular region between 0 and 40 degrees.[17, 18]

The computed data show that when the particle diameter is 3μ, the scattering parameter showing the largest relative change is the scattering efficiency factor Q_s, which lies between one and two, depending on the index of refraction. The extinction efficiency factor Q_e varies by ±10 percent. The phase function decreases by 25 percent with increase in the scattering angle from 0 to 3 degrees. The errors that the uncertainties in the scattering parameters cause in the calculation of the particle densities are discussed in the next section.

3.3 ACCURACY OF MODEL

The average number density of particulates can be computed from a measurement of the directly transmitted laser power. When Equation (18) is substituted in Equation (15), which relates the number density and transmitted power, the average number density is calculated from the following expression:

$$\bar{n} = \frac{\ell n(P(0)/P(L)}{\pi a^2 Q_e L} - \frac{\sigma_{eb} n_b}{\sigma_e} \qquad (21)$$

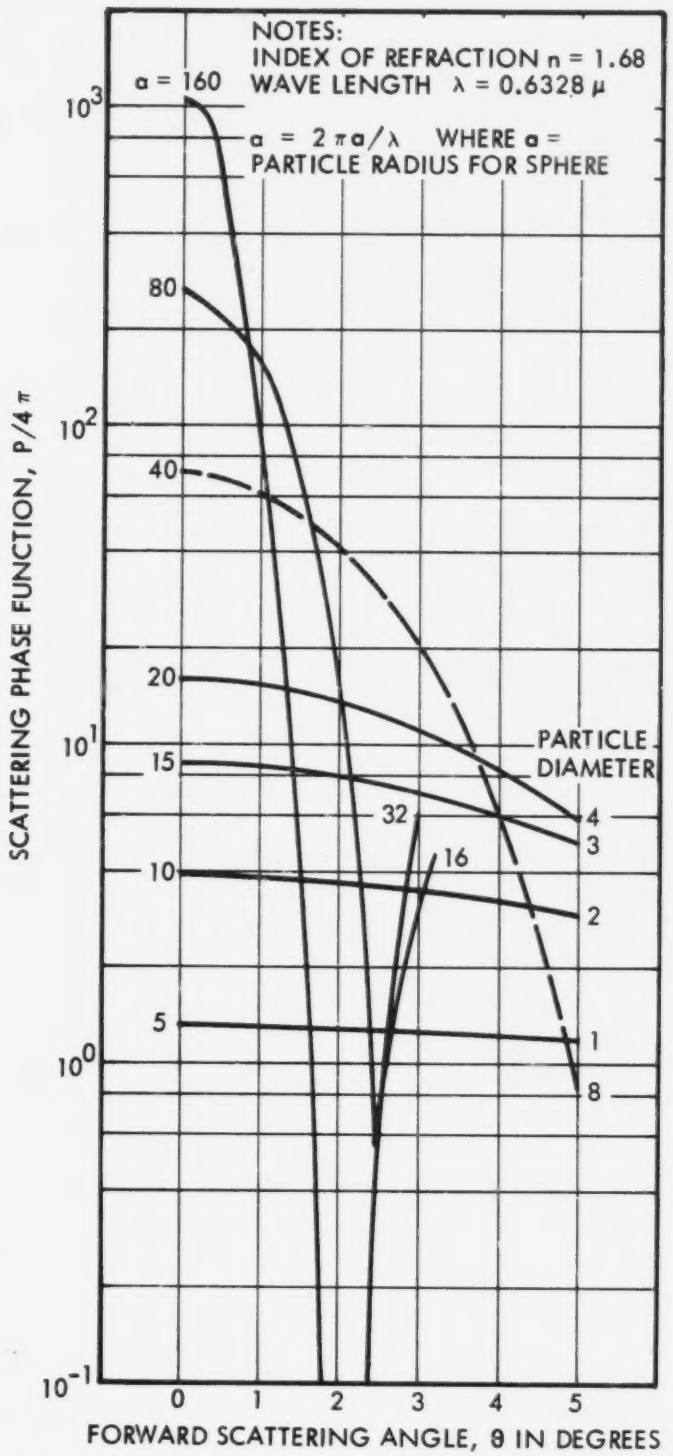

Figure 15. Scattering Phase Function p/4π.

If the background particles cause negligible attenuation, then the relative error in the number density (Δn) is given by

$$\frac{\Delta \bar{n}}{\bar{n}} = \frac{-\Delta P(L) / P(L)}{\ell n\,(P(O)/P(L)} - \frac{2\Delta a}{a} - \frac{\Delta Q_e}{Q_e} \qquad (22)$$

The first term on the right hand side of Equation (22) accounts for the total measurement error. If the transmission is 0.01, then the denominator equals 4.6, and the absolute value of this term should be negligibly small. The relative error in the extinction efficiency factor is ±10 percent. The largest error in the number density may be expected to be caused by the uncertainty in the estimate of the radius.

The relative error in the computed density of limestone precipitated particles can be estimated from Equation (16). In order to simplify the equation, let the geometrical factors be represented by the expression:

$$f(x) = \frac{1}{2\pi\phi^2} \frac{z}{L - x} (r_o + \beta x) \frac{1}{\Delta A} \qquad (23)$$

Substitution of Equations (23) and (18) in Equation (16) yields

$$\epsilon(x) = \frac{f(x)}{a^2 Q_s} \frac{P(x)}{P(0)} \frac{1}{T(L)} \frac{4\pi}{p(\theta(x))}$$

$$- \left[\frac{\ell n(P(0)/P(L)}{\pi a^2 Q_e L} + \left(\frac{\sigma_b}{\sigma} - \frac{\sigma_{eb}}{\sigma_e} \right) n_b \right] \qquad (24)$$

Assume that the measurement errors are negligibly small. Then the relative error in the first term on the right side of Equation (24) is

$$\frac{-2\Delta a}{a} - \frac{\Delta Q_s}{Q_s} - \frac{\Delta P}{P}$$

The relative error in the scattering efficiency (Q_s) can be as large as two. If the particle diameter is 3μ, then an examination of the phase data on Figure 15 shows that the relative error in the phase function approximately equals the relative error in the estimate of the diameters.

If the number of background particles is negligibly small, then the relative error in the second term on the right-hand side of Equation (24) is

$$\frac{-2\Delta a}{a} - \frac{\Delta Q_e}{Q_e}$$

The relative error in Q_e is ±10 percent. The relative error in either the first or second term on the right hand side of Equation (24) depends strongly on the estimate of the particle size, since from this estimate the values of the scattering parameters that are used in Equation (16) are computed.

4. LABORATORY VERIFICATION EXPERIMENTS

To assess the mathematical model described in Section 3, laboratory transmission holography experiments were conducted under relatively controlled conditions using an aerosol of known properties. The scattering chamber described in Section 2. 1. 2 for backscatter experiments was again utilized. The following text describes the test aerosol, transmission holocamera arrangement, hologram data reduction and results. The computer program used in the data reduction is presented in Appendix B.

4. 1 TEST AEROSOL SELECTION AND GENERATION

Several aerosols (Table V), both liquid and dry, were considered as test mediums for transmission holography studies. Samples were taken on microscope slides and photomicrographs made to determine size and shape characteristics. Photomicrographs of religious incense (Figure 5), Unit 10 flyash (Figures 8 through 14) and eraser chalk dust (Figure 3) were illustrated in Section 2. 1. 1 and 3. 2 of this report. Similar photomicrographs of other candidate aerosol materials are illustrated in Figures 16 through 20 of this section of the report. Ultimately, a liquid aerosol, dioctyl phthalate or DOP, was chosen because of the ready availability of data including its index of refraction.

The liquid aerosol generator used for transmission holography experiments was fabricated from a design (Model III) developed by W. H. Eckols and J. A. Young of the U. S. Naval Research Laboratory.[19] The NRL aerosol generator was operated at an inlet pressure of 25 psig.

Table V. List of Candidate Aerosol Materials

Material	Index	Size	Shape	Remarks
Dioctyl Phthalate	1. 48	0. 69μ*	Spherical Drops	
Incense		0. 5 to 2. 0μ	Spherical Drops	See Figure 5
Unit 10 Flyash		1 to 30+μ	Hollow Spheres	See Figures 8-14
Limestone Dust		1 to 10μ	Semi-Spherical	
Pulverized Coal		5 to 250μ	Irregular	No. 60 mesh sample
Chalk Dust		5 to 60μ	Irregular	See Figure 3
Aluminum Oxide		3 to 10μ	Irregular	Alundum Abrasive
Talc, Powder		>60μ	Irregular	J. T. Baker, U. S. P. Talc
Styrene Particles		6 to 14μ	Spherical	Dow Chem. Co.

*Mean Diameter

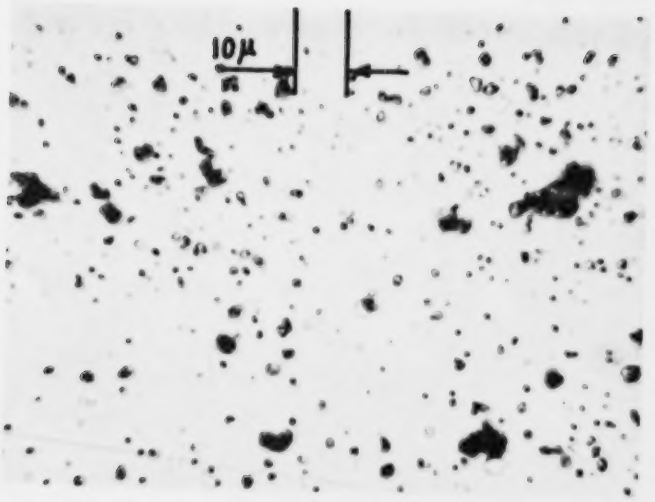

Figure 16. Photomicrograph (60X) of pulverized limestone sample from Unit 10 limestone injection system. (Sample taken on 12 March 1970).

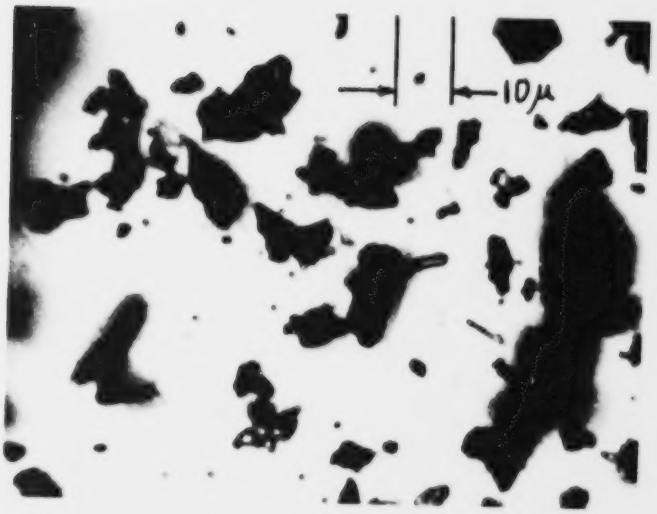

Figure 17. Photomicrograph (60X) of No. 60 mesh (250μ) pulverized coal sample from Unit 10.

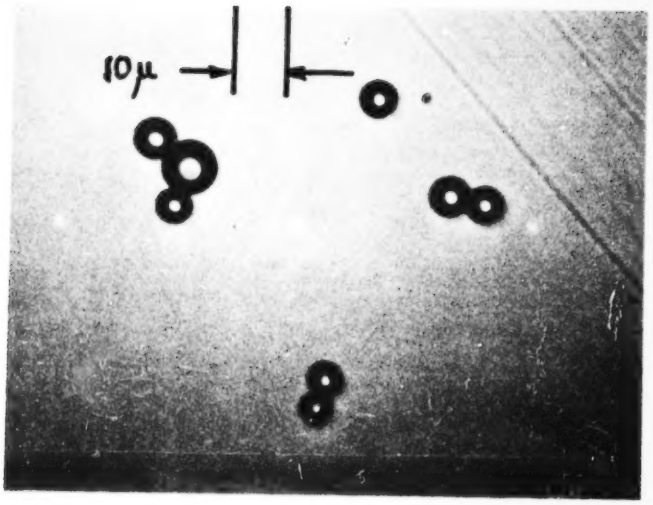

Figure 20. Photomicrograph (60X) of Dow Chemical Co. Styrene divinyl benzene spheres. Nominal size indicated to be 6.7 microns.

In the original work by Eckols and Young, a light scattering photometer was used to determine mean aerosol particle diameter as a function of DOP mass flow rate for various generator inlet pressures. At an inlet pressure of 25 psig, the mean droplet diameter was found to be 0.69 micron. Direct measurement of aerosol droplet size distribution was not made during the present work; however, aerosol mass flow rate was measured (for an inlet pressure of 25 psig) and compared with the published results. Close agreement was obtained and therefore, the published droplet mean diameter of 0.69 micron was accepted as a reasonable approximation.

Some holograms were also recorded of dry (Unit 10 flyash) aerosols and of particulate and smoke produced by combusting metal-loaded solid rocket propellant samples. * The dry aerosol was produced using a Crider Dust Feeder.[20]** The solid rocket propellant samples were ignited and burned at one atmosphere. The resulting combustion produced a shower of large aluminum oxide (Al_2O_3) particles accompanied by dense acrid smoke.

4.2 TRANSMISSION HOLOCAMERA APPARATUS

The transmission holocamera used to record low angle forward scattering is shown schematically in Figure 21. As in previous

---

*Ammonium perchlorate (NH_4ClO_4) and aluminum particles in an epoxy binder.

**Information on the Criter Dust Feeder was provided by Mr. D. K. Felton of APCO/DPCE.

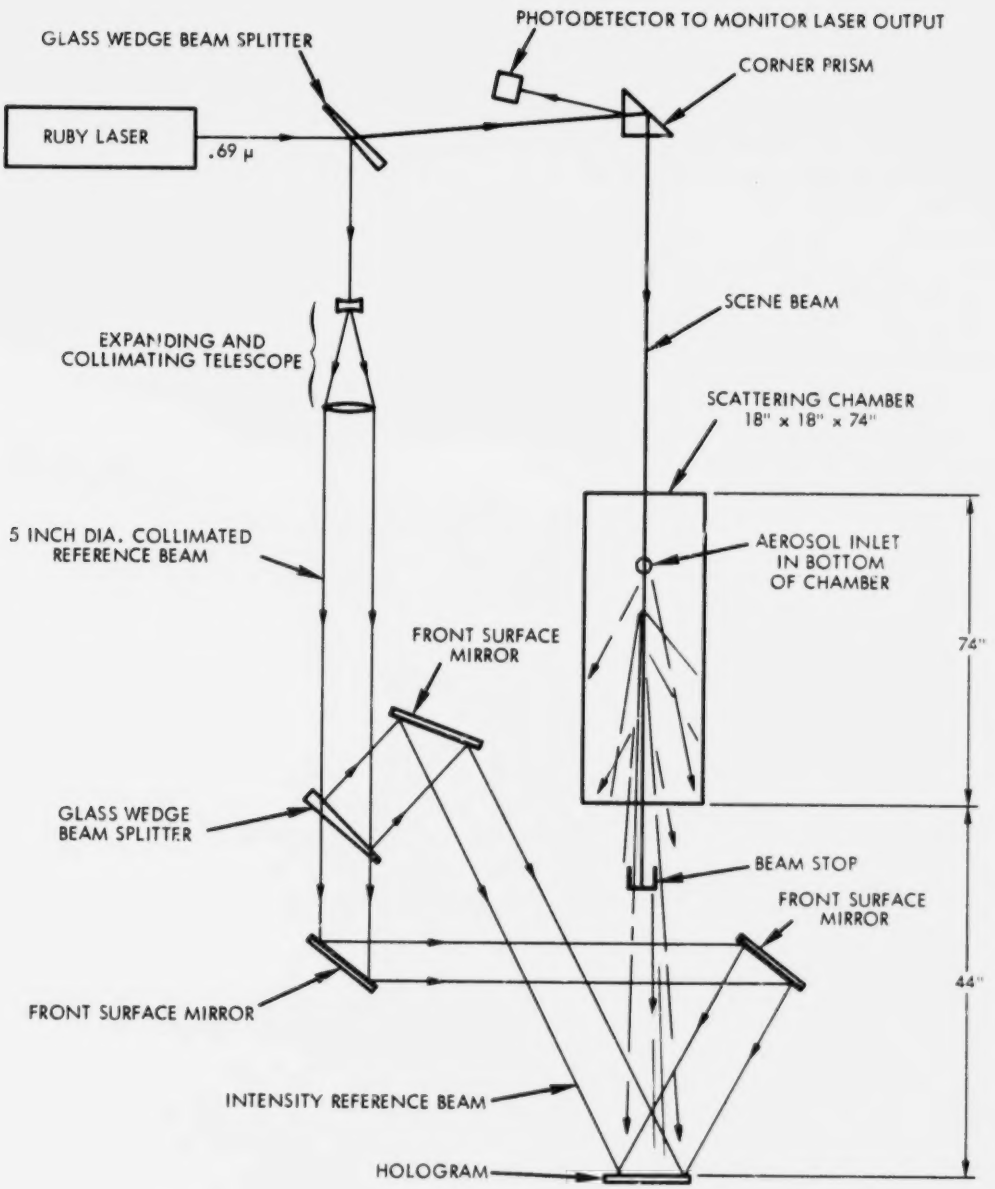

Figure 21. Schematic diagram of scattered light three-beam transmission holocamera test setup.

transmission holocamera arrangements for recording forward scatter, the 0.69 micron ruby laser output is initially divided into an unexpanded scene beam and an expanded and collimated 5-inch diameter reference beam. * The 5/8-inch diameter scene beam is directed through the scattering chamber via a corner prism. Scene beam divergence through the 74-inch length of the scattering chamber is negligible. The ruby scene beam does not impinge on the holographic film plate. Only low angle forward scattering of the scene beam is received by the hologram. Recombination of scattered scene light and reference illumination at the plane of the holocamera results in constructive and destructive interference of the two wavefronts. The holographic plate records the intensity distribution due to the interference phenomenon.

The unique and new feature of the present holocamera arrangement is the addition of a second reference beam resulting in a "three-beam" system. (This arrangement was initially described in Section 2.4 in an evaluation of the potential of the backscatter technique.) The second reference beam is generated by adding a glass wedge beam splitter in the path of the original reference beam. From Figure 21 it will be seen that front surface mirrors direct both reference beams onto the holographic plate.

The second reference beam provides a point of reference light intensity within the reconstructed hologram which may be subsequently measured and related to the incident laser scene beam energy. The incorporation of a second reference beam is important for another reason; namely, a hologram is recorded even though the scene beam may be heavily (or completely) attenuated. ** Reconstruction and observation of very weak scene beam signals can be accomplished.

The laser illuminator used for the transmission holography was a conventional Q-switched ruby oscillator with a single ruby amplifier. It is the same TRW illuminator used previously at the Shawnee Steam Plant in the holography of injected limestone plumes. A minor modification was made in that the silicon photodiode used to monitor the relative

---

*See Reference 1 for description of earlier two-beam transmission holocamera. In particular, refer to pages 18 through 23.

**In conventional two-beam holocameras, heavy absorption or scattering of the scene beam necessitates a corresponding attenuation of the reference beam to preserve a desired 1:1 to 1:4 scene/reference beam intensity ratio.[21] Diminished light intensity at the hologram can result in adverse exposures at the low non-linear end of the film emulsion characteristic curve. Conversely, a three-beam system eleviates the necessity of closely matching scene/reference beam intensity ratios. Proper exposure of the hologram is accomplished via the two reference beams. The weak scene illumination modulates the simple interference pattern established by the two reference beams. As reported by Heflinger and Brooks in Reference 6, the scene light intensity may be attenuated by a factor of 10^{-6} over the reference beam intensity and still be observed in the reconstructed homogram.

emission of the ruby oscillator was removed from the laser cabinet. The photodiode was mounted external to the laser such that total emission (oscillator plus amplifier) could be monitored. A reflected beam from the first surface of the corner prism (Figure 21) was used for this purpose. The photodiode was calibrated using a TRG Ballistic Thermopile to measure the absolute output of the laser. * The laser output was typically 1. 52 to 1. 58 joules.

4. 3 FORWARD SCATTER HOLOGRAPHY AND RECONSTRUCTION

Eighteen forward scatter holograms (Table VI) were made during the final part of the test program including recordings of chalk dust, metal-loaded solid rocket propellant specimens, Unit 10 flyash and DOP aerosol. All recordings were made using Agfa 8E75 emulsion on 4 x 5-inch glass plate. With the exception of the initial four holograms, laser light attenuation measurements were made immediately after each recording. This was accomplished using a Spectra Physics Model 124-A continuous wave helium-neon gas laser (0. 63 micron) and Model 401 power meter.

The Spectra Physics helium-neon gas laser was also used to reconstruct the scattered light holograms. Each hologram to be evaluated was carefully oriented before a collimated 2-inch diameter beam so that the real image was projected in space. The method of reconstruction is shown in Figure 22. In projecting and measuring scattered light intensity variations of the real image, the intermediate step of photographing the reconstructed virtual image (before further data processing) is eliminated. ** Image location (distance) measurements are made directly rather than by angular measurement as in the previous work (see Reference 1). Direct measurement of both image intensity and distance eliminates potential error which may be introduced via the intermediate photographic process.

With the hologram illuminated by a continuous wave gas laser, two beams of light emerge which are of interest. One is the reconstructed scene beam real image and the other is the second reference light intensity beam (Figures 21 and 22). The emerging reference intensity beam is brought to focus with the aid of a 5-inch diameter, 24-inch focal length lens. The total flux of the beam is directed into a 20 mm^2 aperture on a monitoring photodetector. A portable photodensitometer is used to measure the light intensity. *** At this point the scale on the densitometer is adjusted to read 100 percent.

---

*TRG Model 107 Ballistic Thermopile, Hadron, Inc., Westbury, N. Y.

**In the previous work (described on pages 25-26 and 42-54 of Reference 1, a photographic negative of the hologram virtual scattered light image was made. Variations in image intensity (as recorded on the photographic negative) were then measured using a microdensitometer.

***Photovolt Corp. Model 520A Photodensitometer.

Table VI. Summary of Low Angle Forward Scattering Ruby Laser Transmission Holograms

Date	Record No.	Test Scene	I/I_o	Devel. Time	Remarks
8-4-70	1	Chalk Dust		2.5 min.	Prelim. test, good reconstruction scene/Ref. ~1/4.
	2	Solid Propellant		8	Plate fogged.
	3	Solid Propellant			Hologram of rocket propellant smoke (Post combustion).
	4	Solid Propellant			Same as 8-4-70, #3.
8-10-70	1760	Empty Chamber	1.00		Good quality reconstruction
	1761	DOP Aerosol	0.59	6	Aerosol generator at 25 psig; laser beam divergence ~0.
	1771	DOP Aerosol	0.3		Laser amplifier out, good hologram
	1772	DOP Aerosol	0.35		Same as #1771
	1773	Empty Chamber	1.00		Good hologram
	1774	DOP Aerosol	0.90		Osc. only, recorded early in 5 sec duration DOP generation. Good hologram.
	1776	DOP Aerosol	0.83		Same as #1774.
	1777	DOP Aerosol	0.66		12 sec burst of DOP.
	1778	3 to 30μ Flyash	0.66		Used Crider dust generator at inlet press. of 35 psig. Good hologram.
	1779	3 to 30μ Flyash	0.78		Same as #1778.
8-11-70	1781	DOP Aerosol	0.78	3 min.	10 sec burst of aerosol, recording made at end of aerosol injection
	1782	DOP Aerosol	0.61		Second recording of #1781 aerosol injection
	1783	DOP Aerosol	0.61		20 sec burst of aerosol, recording made at end of aerosol injection.
	1784	DOP Aerosol	0.72		Second recording of #1783 aerosol injection.

The photodetector is next placed on an optical rail and aligned such that the 20 mm^2 aperture receives the focused scattered light image at any given focal position along the scene beam optical path. Location of the scattering chamber relative to the holocamera film plate is known; therefore, the ends of the chamber can be defined with respect to the projected real image. It was also possible to locate an image of the laser beam entry port at the far end of the scattering chamber in the reconstructed scene. This provided a distance calibration measurement.

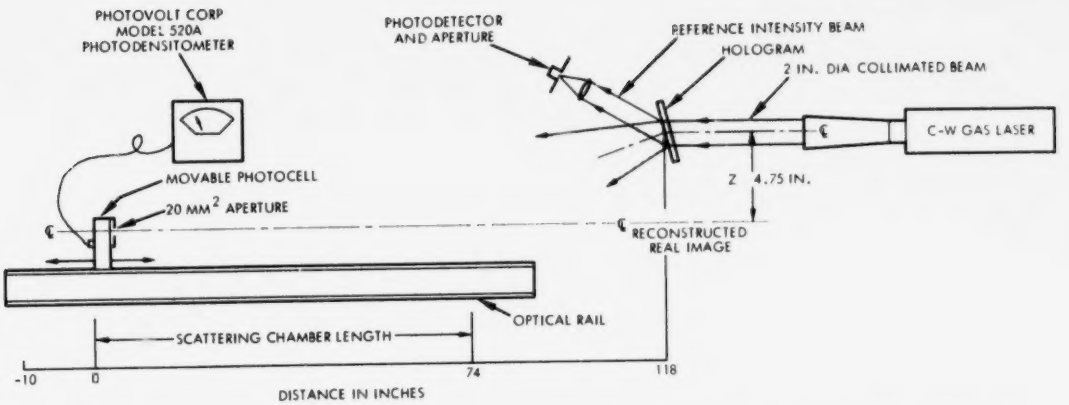

Figure 22. Schematic diagram of method used to reconstruct and measure hologram real image light intensity variations as a function of scattering chamber length.

With the photodetector properly aligned, scene beam light intensity measurements were recorded at 3-inch intervals along the optical path. Since the photodensitometer scale was previously adjusted to 100 percent (full scale) for the total flux of the reference intensity beam, all scene beam intensity measurements were therefore proportional. The relationship of the reference beam intensity to the incident pulsed ruby laser beam intensity was determined separately, and is a fixed constant for this holocamera. The helium-neon alignment laser in the pulsed ruby laser system was turned on and sent through the holocamera (Figure 21). The photodetector (with 20 mm^2 aperture) was placed before the holocamera scene beam and the photodensitometer scale again adjusted to a full scale reading of 100 percent. Next, the second reference beam from the beam splitter (Figure 21) was apertured to a 2-inch diameter. This diameter was equivalent to that of the reconstruction gas laser collimated beam. The second reference beam was subsequently focused to a point using a 5-inch diameter, 24-inch focal length lens. The photodetector was positioned at the focal point and the intensity of the reference beam measured and found to be 0.175 percent. This value then, is a correction factor which relates the measured reconstructed image intensity to the incident ruby laser intensity:

$$\text{Reconstruction measurement} = \frac{I_{scene}}{I'_{ref.}} \times \frac{I_{ref}}{I_o}$$

$$= \frac{I_{scene}}{I_o} \times 0.00175$$

where

I_{scene} = Reconstructed scene intensity

I'_{ref} = Reconstructed reference beam intensity set equal to 100 percent

I_{ref} = Measured holocamera reference beam intensity

I_o = Incident laser beam intensity set equal to 100 percent

Using the procedure described, six holograms were reconstructed and measured for light intensity variation as a function of distance. The reconstructed holograms were numbers 9-4-70 -#1, #1771. and #1781 through #1784. Image intensity data from holograms #1781-1784 were processed to determine particle number density information.

4. 4 HOLOGRAM DATA REDUCTION

Equation (2) formulated by R. S. Fraser in Section 3. 1 relates the ratio of scattered light power received by an element of the hologram to the incident ruby laser power:

$$\frac{P(x)}{P_o} = T(x)T(y)\,\Delta V(x)\,\frac{n(x)\sigma}{\Sigma(x)}\,p\,\frac{(\theta(x))}{4\pi}\,\frac{\Delta A}{|y(x)|^2} = I(x) \qquad (2)$$

In this equation, the scattering cross-section per unit volume $n(x)\sigma$ consists of two terms to account for the laser scatter due to injected limestone particles and the boiler flyash. Equation (11) of Section 3. 1 expressed this quantity as:

$$n\sigma = (\bar{n} + \epsilon)\,\sigma_\ell + n_b\sigma_b \qquad (11)$$

where the subscripts ℓ and b refer to the limestone and boiler flyash, respectively. From Equation (10) it will be recalled that $\bar{\epsilon}$, the deviation of the density of injected limestone particles from the average is zero for the path L of the laser scene beam.

$$\bar{\epsilon} = L^{-1}\int_o^L \epsilon\,(x)\,dx = 0 \qquad (10)$$

When a background of flyash and a quantity of injected limestone are both present, two transmission measurements are required to determine number densities. The average for flyash is obtained from a transmission measurement T_1 taken with no limestone injection, using Equation (13).

Equation (14) shows the transmission measurement T_2 to be a product of T_1 and the attenuation due to limestone, so that the average limestone number density is computed from the ratio T_2/T_1 using Equation (15). For the present laboratory tests there was no flyash present ($n_b = 0$) and hence, T_1 = unity. Consequently, n refers only to the DOP aerosol and $\bar{n}$ can be determined from a single transmission measurement:

$$\bar{n} = \frac{-1}{\sigma_\ell L} \ln \left(\frac{P}{P_o}\right) \tag{25}$$

From the hologram reconstruction technique used in the laboratory tests:

$$\theta = \tan^{-1} (z/(L - x), \tag{26}$$

$$y = \frac{L - x}{\cos \theta} \tag{27}$$

and the elemental volume

$$\Delta V = W^2 (2r_o) \frac{1}{\sin \theta}, \tag{28}$$

where θ, z, y, L and x are geometric terms defined by the schematic diagram of Figure 23. W is the dimension of the square aperture of the photodetector and r_o is the radius of the incident ruby laser beam.

From the preceding discussion, the scattering cross-section per unit volume may now be written as:

$$n(x)\,\sigma = \frac{T(x)}{T(L)} \quad \frac{\Sigma}{\Delta V} \frac{4\pi}{p} \frac{y^2}{\Delta A} \tag{29}$$

The term Σ was previously defined as the area of the laser beam cross-section normal to the beam (x) axis:

$$\Sigma (x) = \pi r^2 = \pi (r_o + \beta x)^2 \tag{5}$$

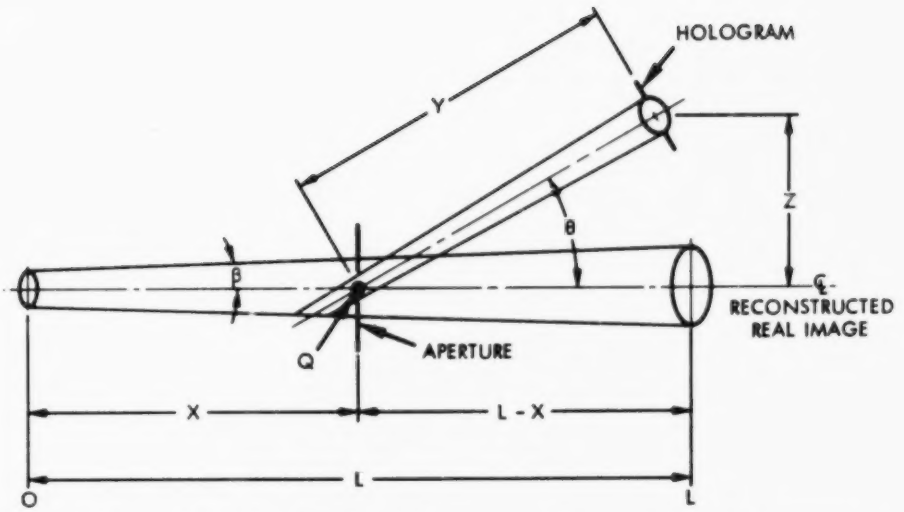

Figure 23. Schematic diagram of reconstructed scene beam real image, hologram and photodetector aperture. Diagram is oriented to coincide with sketch of hologram reconstruction setup shown in Figure 22.

From Section 3.1, β was defined as the ruby laser beam divergence through the aerosol, or $\beta = dr/dx$. The aerosol particle density deviation may now be expressed as:

$$\epsilon(x) = \frac{1}{\sigma_\ell}\left[I(x)\frac{1}{T}\,\frac{\pi(r_o+\beta x)^2\sin\theta}{W^2 2r_o}\,\frac{(L-x)^2}{(\cos\theta)^2}\cdot\frac{4\pi}{p\Delta A} - (\bar{n}\sigma_\ell + n_b\sigma_b)\right] \qquad (30)$$

For the laboratory tests, Equation (30) may be further simplified. Ruby laser beam divergence through the 74-inch long scattering chamber DOP aerosol was measured and found to be negligible; therefore, $\beta = 0$. Further, there was no flyash background particulate so that $n_b\sigma_b = 0$. The scattering phase function $p/4\pi$ was assumed to be unity for the laboratory tests. Referring to Figure 15, it will be seen that for particle mean diameters of the order of 1 micron or less, $p/4\pi$ is very close to one.

Estimates of DOP aerosol particle number density as a function of distance along the x-axis (reconstructed scene beam) may now be

determined by substituting Equations (25) and (30) into Equation (11) and solving for n. The resulting equation is:

$$n(x) = I(x) \left(\frac{\pi r_o^2 z}{T \sigma_\ell 2W^2 \Delta A} \right) \left(\frac{L - x}{\cos \theta} \right) \tag{31}$$

Input Data | Constants | f(x)

From this equation it will be seen that the first term represents the scattered light intensity measurements obtained from the reconstructed scene. All of the constants for a given test have been lumped into the second term. The third term of Equation (31) contains the geometric variables of x. The computer program designed to process data with Equation (31) is presented in Appendix B.

4.5 EXPERIMENTAL RESULTS

Using the NRL liquid aerosol generator (Reference 19), dioctyl phthalate (DOP) fog was introduced into the scattering chamber for a period of 10 seconds. The aerosol was allowed to diffuse throughout the chamber for ~3 minutes. Assuming a monodisperse aerosol with each particle having a 0.69μ diameter, there were approximately 1.4×10^{11} particles injected into the scattering chamber (Appendix C). If it is further assumed that the aerosol particles were uniformly distributed throughout the scattering chamber without any losses, the particle number density n would have been $\sim 5.8 \times 10^6$ particles/in.^{3}.

Hologram numbers 1781 and 1782 were recorded after the initial injection of DOP into the chamber. Another 10 second injection of DOP was made followed by the recording of two additional holograms (1783 and 1784). Using the simplifying assumptions as before, the number density n would equal $\sim 11.6 \times 10^6$ particles/in.^{3} after the second aerosol injection. *

The four test holograms were developed, reconstructed and reduced for data using the methods described in Sections 4.3 and 4.4. Accordingly, particle number densities for holograms 1781 through 1784 are presented graphically in Figures 24 through 27, respectively. Note that in each case, the particle density (n, particles/in.^{3}) data points extend

---

*The assumptions over simplify the aerosol density and distribution in the scattering chamber; however, such calculations yield rough approximations independent of any optical measurements. They are useful in comparing with the results obtained via holography and the simple transmission measurements.

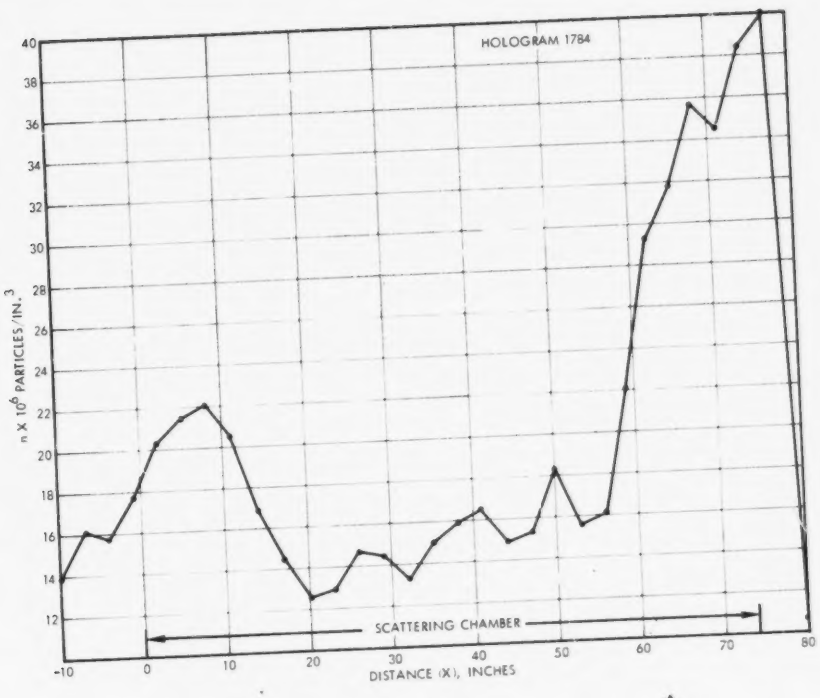

Figure 27. Particle number density versus distance for hologram 1784

beyond the ends of the 74-inch long scattering chamber. Both acrylic end pieces of the chamber contained 1.5-inch diameter holes through which the pulsed ruby laser beam passed. This eliminated confusing beam reflections from the acrylic surfaces. Some aerosol drifted out of the scattering chamber during each test. The scattered light image on either side of the chamber was measured for intensity during the real image data acquisition and the resulting data was incorporated in the plots.

The data for hologram 1781 (Figure 24) indicates that the aerosol was quite uniformly distributed along the beam path. The distribution remained uniform during hologram 1782 (Figure 25) with the exception that some eddies apparently shifted the aerosol concentration toward the right side of the box. This same trend is noted in recordings 1783 and 1784. This end of the scattering chamber was opened and closed during each hologram recording cycle and may well account for the variations in local particle number densities.

As noted earlier, additional DOP was injected into the scattering chamber before holograms 1783 and 1784 were recorded. This is reflected in the increased number densities shown in Figures 26 and 27. Theoretically, the particle number density increased by a factor of ~2 after the second injection of DOP for an average value of $n = 11.6 \times 10^6$ particles/in.^{3}. The increase in n is very evident when comparing holograms 1781 and 1782 with 1783 (Figures 24 and 25 with Figure 26). An apparent loss of DOP from the chamber occurred between holograms 1783 and 1784 (Figures 26 and 27). As noted previously, there is a strong concentration of aerosol on the right-hand side of the scattering chamber evidently from an air current. A trend of this nature appears to have begun at the time of recording hologram 1782 (Figure 25), and subsequently increased during the next two recordings (Figures 26 and 27).

A summary of calculated and measured mean particle number densities for each of the reduced holograms is shown in Table VII. The calculated $\bar{n}_C$ (Appendix C) is an estimate of average particle density which is independent of any optical measurement. It is, therefore, a useful check against unreasonable results obtained via holographic and light transmission measurements. The calculated $\bar{n}_C$ is a factor of 10 greater than the measured values of $\bar{n}_\ell$ and $\bar{n}$. This is due to simplifying assumptions used in the calculation of $\bar{n}_C$; namely, a monodisperse aerosol uniformly distributed without any losses.

Values for "Measured $\bar{n}_\ell$" in Table VII represent averages (using the trapezoidal rule) of the data presented in the plots of Figures 24 through 27. The "Measured $\bar{n}$" values are based upon transmission measurements (Equation 3) made concurrently with the respective hologram recordings. For average values of n, the transmission measurement data are considered as the standard for comparison. The right-hand column in Table VII compares the scattered light hologram data to the transmission measurements. The results are quite favorable. The average values of $\bar{n}$ obtained from hologram data are within a factor of approximately 2 from the transmission measurements. Also significant in the Table VII summary is the narrow range (1.29 to 2.51) between the four $\bar{n}/\bar{n}_\ell$ values.

Table VII. Comparison of Calculated and Measured Values of $\bar{n}$

Hologram No.	Calc. $\bar{n}_c$ (Particles/in.^{3})	Meas. $\bar{n}_\ell$ (Particles/in.^{3})	Meas. $\bar{n}$ (Particles/in.^{3})	Ratio $\bar{n}/\bar{n}_\ell$
1781	$\sim 5.8 \times 10^6$	8.47×10^5	16.37×10^5	1.93
1782		7.29×10^5	11.87×10^5	1.63
1783	$\sim 11.6 \times 10^6$	24.87×10^5	32.08×10^5	1.29
1784		8.42×10^5	21.20×10^5	2.51

Notes:
1) Calc. $\bar{n}_c$ = Theoretical calculation independent of optical measurements (Appendix C).
2) Meas. $\bar{n}_\ell$ = Average value of particle density calculated from hologram reconstruction intensity measurements $(P(X)/P_o)$
3) Meas. $\bar{n}$ = Lambert-Beer calculation from gas laser transmission measurements.

It is thought that differences between corresponding values of $\bar{n}$ and $\bar{n}_\ell$ (Table VII) are due to assumptions made while deriving and applying Equation (31) to the calculation of n(x). In particular, it was assumed that the scattering phase function $p/4\pi$ was unity, ruby laser beam divergence β was negligible, and that the value for the scattering cross-section σ_ℓ was representative for the test aerosol. A single value of σ_ℓ implies a monodisperse aerosol (which was not the case for the present tests) or an aerosol whose size distribution can be adequately characterized by a mean particle diameter. For the laboratory tests, the value of σ_ℓ contains a greater degree of uncertainty since the aerosol size distribution was not measured directly.

Another objective of the experimental work was the determination of practical size limits on particles which may be detected via scattered light holography. Time and funding limitations did not permit a systematic investigation to determine limits on particle size, scene light attenuation, available ruby laser energy, etc. It should be noted, however, that scattering of the ruby laser beam by smokes with particle diameters less than 1 micron were successfully recorded via holography. Based upon physical reasoning, it would seem probable that the basic technique could be extended to even smaller particles.

5. CONCLUSIONS

From the experimental work conducted during this program, the following conclusions have been reached:

- Holography of ruby laser back scatter is feasible and might be utilized for investigations at the Shawnee Unit 10 boiler.

  (1) The success of the back scatter technique is due to the TRW developed chlorophyll dye cell laser.

  (2) Observable scene depths are strongly dependent on the optical "thickness" of the aerosol.

  (3) Optical ranging of aerosol clouds is possible within the observable scene depth.

  (4) A preliminary evaluation of back scatter mathematical modeling indicates that it is feasible; however, the results will probably be less accurate than for low angle forward scatter.

- The mathematical model derived for low angle forward scatter yields average particle number density estimates within a factor of ~2 for similar values obtained via simple transmission measurements. The present model is valid only for:

  (1) Low angle forward scattering and known geometries.

  (2) Holograms which include a reference intensity calibration.

  (3) Aerosols which may be characterized by a mean particle diameter and refractive index.

  (4) Holograms recorded concurrently with an aerosol scene transmission measurement.

- Real image reconstruction of low angle forward scatter holograms proved to be a more accurate and convenient method of acquiring scene data.

  (1) Direct image distance measurements were made.

  (2) Hologram calibration was preserved, hence, absolute light intensities could be measured and data from successive recordings could be compared.

  (3) The intermediate and less accurate photographic step was eliminated.

(4) Interrogation of the hologram real image could, if desired, be fully automated.

- Computer programming of the mathematical model was accomplished and applied to the data reduction of scattered light intensity measurements.

- Data reduction methods developed for the laboratory tests may be utilized for "on-site" data processing at the Shawnee Unit 10 boiler.

- Limitations on particle size with respect to the scattered light holography technique were not fully explored; however, smoke particles corresponding to the wavelength of ruby light (0.69μ) were recorded at ranges up to 6 feet.

6. RECOMMENDATIONS

The use of back scatter ruby laser holography should be explored and developed to define the extent that quantitative data on particle density measurements can be made.

Systematic investigations should be made to determine particle size limitations for both the forward and back scatter holography techniques.

Work should be initiated to develop methods for making particle size measurements using both scattered light holography and multiple color direct laser scattering techniques.

NOMENCLATURE

Q	point at (x, 0)	
x	x, dist variable	(in.)
L	x dist to hologram, and end of scattering volume	(in.)
z	verticle distance	(in.)
y	path length, Q to (L, z)	(in.)
θ	scattering L to hologram	
p	power in laser beam	(w)
T	transmission factor	
n	number density	(particles/$in.^3$)
V	volume element in vicinity of Q	($in.^3$)
σ	cross section for light extinction	($in.^2$)
Σ	cross section of laser beam	($in.^2$)
p	scattering probability factor at angle θ	
ΔA	area element at hologram (or illuminated area of hologram)	($in.^2$)
n_b	flyash density	
$\bar{n}$	average limestone density	
n_ℓ	actual limestone density	
ϵ	variation from average ($\bar{n}$)	

REFERENCES

1. B. J. Matthews and R. F. Kemp, "Holographic Determination of Injected Limestone in Unit 10 of the Shawnee Power Plant," Final Report, TRW No. 14103-6001-R0-000, June 1970, pp. 12-14.

2. R. F. Wuerker, "Instruction Manual for Ruby Laser Holographic Illuminator," TRW Report No. 11709-6003-R0-00 (AFRPL Contract F04611-69-C-0015), February 1970. In particular, refer to discussions on ruby laser coherence (pp. 22-30) and dye cells (pp. 113-114).

3. R. F. Wuerker and L. O. Heflinger, "Laser Holography Study," Final Report for the Air Force Avionics Laboratory, Wright-Patterson Air Force Base, July 1970 (in preparation).

4. B. J. Matthews and R. F. Kemp, Op. cit., pp. 25-26.

5. Robert Hickling, "Holography of Liquid Droplets," Research Publication GMR-869, Research Laboratories, General Motors Corp., Warren, Michigan, April 1969.

6. Lee O. Heflinger and Robert E. Brooks, "Holographic Instrumentation Studies," Final Report under NASA Contract No. NAS 2-4992 (TRW Report No. 12122-6007-R0-00), September 1970, pp. 5-9 (in preparation).

7. B. J. Matthews, R. F. Wuerker and R. F. Kemp, "Holographic Determination of Injected Limestone Distribution in Unit 10 of the Shawnee Power Plant," TRW Progress Report No. 1170.69-001, September 1969, pp. 6-8.

8. Private communication from D. T. Clay, 17 March 1970. See also Tennessee Valley Authority Report No. 54 covering test results of the period 9 July - 6 August 1969.

9. Ibid.

10. J. R. Hodkinson, in: Electromagnetic Scattering, ed. by M. Kerker (Pergamon Press, New York, 1963), pp. 87-100.

11. A. C. Holland and G. Gagne, "The Scattering of Polarized Light by Polydisperse Systems of Irregular Particles," Applied Optics 9, 1113 (1970).

12. Walter C. McCrone, in: Air Pollution, Vol. II, ed by Arthur C. Stern (Academic Press, New York, 1968), p. 301.

13. Otto de Lorenzi, ed., Combustion Engineering, (Combustion Engineering Inc., New York, 1955), pp. 2-28 and 2-29.

14. J. S. Morris, "Dry Limestone Injection Process for SO_2 Control," (Part IV - Solid Waste and Water Quality Considerations), Paper presented at the NAPCA Symposium on the Dry Limestone Injection Process, Gilbertsville, Kentucky, June 1970.

15. Walter C. McCrone, Op. cit, p. 288.

16. Charles D. Hodgman, ed., Handbook of Chemistry and Physics, 40th Edition (The Chemical Rubber Publishing Co., Cleveland, Ohio, 1959) p. 2932.

17. J. D. Hodkinson, op. cit.

18. A. C. Holland and G. Gagne, op. cit.

19. W. H. Eckols and J. A. Young, "Studies of Portable Air-Operated Aerosol Generators," U. S. Naval Research Laboratory, Report No. 5929, 26 July 1963.

20. J. W. Davis and R. L. Byers, "Characteristics of a Dry Dust Aerosol Generator," Paper presented at the 62nd Annual Meeting of the Air Pollution Control Association, New York, New York, June 1969.

21. R. F. Wuerker, "Operational Manual for Transmission Holocamera," AFRPL Contract F04611-69-C-0015, TRW Report No. 11709-6002-R0-00, February 1970, p. 15.

APPENDIX A

Appendix A

The Imaginary Part of the Index of Refraction

If the index of refraction has an imaginary part, the propagation of light is altered. It will be quickly shown that the imaginary part represents an attenuation on a light wave passing through a media of index n.

In its simplist form the propagation of light may be expressed as:

$$\text{Wave} = A_o e^{\,j(\omega t - kx)} \tag{1}$$

where,

A_o	is the amplitude of the light wave
e	is the base of the natural system of logarithms
j	is $\sqrt{-1}$
ω	is the angular frequency f of the wave in radians per unit time ($\omega = 2\pi f$)
t	is time
k	is the wave number (i.e., $k = 2\pi/\lambda$)
x	is distance

The equation represents a wave moving to the right at a constant velocity. This can be seen by setting the argument of the exponent equal to a constant; namely, $\omega t - kx$ = constant. Differentiating x with respect to t one obtains $dx/dt \equiv C$. In vacuum, the index of refraction is unity. When light moves through a media of refractive index not equal to unity, the wave velocity slows. The index n is related to the velocity v by the following: $v = c/n$. By substitution, one can write the original equation in terms of n:

$$\begin{aligned} \text{Wave} &= A_o e^{\,j(\omega t - n\omega x/c)} \\ &= A_o e^{\,j(t - nx/c)\omega} \end{aligned} \tag{2}$$

Now let $n = n_o - j\Delta$ so that the index of refraction contains both a real (n_o) and an imaginary ($j\Delta$) part. The symbol Δ represents the numerical value of the imaginary part. Again, by substitution,

$$\text{Wave} = A_o e^{\,j(t-n_o x/c + j\Delta x/c)}$$

$$= A_o e^{\,-(\Delta\omega/c)x} \quad e^{\,j(t-n_o x/c)\omega} \qquad (3)$$

Inspection of Equation (3) shows that it now contains a term $A_o e^{-(\Delta\omega/c)x}$. This quantity represents an attenuation of the wave amplitude as the distance x increases. This occurred due to the imaginary part of the index. The attenuation is multiplied by the function $e^{\,j(t-n_o x/c)\omega}$, which has already been shown to be the expression for a right traveling wave (Equation 1). The wave moves to the right at a velocity $dx/dt = v = c/n_o$.

In essence, the real part of the refractive index determines the speed of light through a given media while the imaginary part imposes a damping effect on the light wave resulting in attenuation or absorption of the wave energy.

APPENDIX B

Appendix B

Computer Program

The computer program shown in Figure B-1, was written and used to demonstrate the feasibility of computer assisted data reduction of information from reconstructed holograms. A brief description of the program follows, covering in particular the translation between the equations given in this report and the various identifiers and operations in the program. Following this, the next steps in up-grading the program are identified.

A simplified version of Fraser's equation, Equation (31), has been coded in the FORTRAN IV language. The first line (PROGRAM card) is unique to the CDC 6000 series computers, otherwise the program will run on any computer having FORTRAN IV capability. The listing was prepared on a standard teletype machine, communicated to the TRW Time-Sharing Service (CDC 6400) and operated via telephone line. Comparative nomenclature for program identifiers and the symbols in Equation (31) are shown on the following page. When it is run, the program first computes number density estimates based on the table of input values. It then computes the average of these based on a trapezoid-rule integration and compares this with an average computed from a light-transmission measurement. The values for number density printed out are those normalized to the transmission measurement.

For use in data reduction from Shawnee, the program can be operated from a standard teletype machine installed at the plant. Some changes will need to be incorporated in the program to take care of two transmission measurements instead of one, to accommodate an anticipated change in aperture shape, and to incorporate the probability factor p/4n (probably as a function subroutine).

$$n(x) = I(x) \left(\frac{zr_o}{T\sigma 2W^2\Delta A}\right)\left(\frac{L-x}{\cos\theta}\right) \qquad (31)$$

Nomenclature:

Equation (31)		Program Listing
x	distance along beam axis	x
n(x)	number density estimates	DENS (i) i = 1, N
I(x)	hologram image intensities	P (i) i = 1, N
T	ratio of two power meter readings	T_1 (box empty) T_2 (aerosol present)
r_o	laser beam radius	RO
z	distance, hologram to beam axis	Z
L	distance, hologram to scene end	BL
W	width of square scanning aperture	W
ΔA	illuminated hologram area	DA
$p/4\pi$ (Eq. 30)	scattering probability factor	PRF
σ_ℓ	limestone scattering cross section	SL
--	program control flow flag	F1
--	factor of input constants	F2
--	increment in x-distance	Dx
θ	scattering angle	TH
--	average density from first computation	BN1
--	" " " transmission measurement	BN2

Figure B-1

```
      PROGRAM LIME (INPUT,OUTPUT,TAPE5=INPUT,TAPE6=OUTPUT)
C  COMPUTES LIMESTONE PARTICLE NUMBER DENSITY ESTIMATES FROM
C  HOLOGRAM DATA.
C  DIMENSIONS IN INCHES
      DIMENSION P(100),DENS(100),XI(100)
      NAMELIST /INP/T1,T2,RO,Z,BL,W,DA,SL,P,F1,N,DX,NO
C  DEFAULT VALUES
      T1=1.
      T2=T1
      RO=.25
      Z=4.75
      BL=129.
      W=.176
      DA=3.14159
      PRF=1.
      SL=1.19E-9
C  READ INPUT AND COMPUTE ESTIMATES
    1 F1=1.
      READ(5,INP)
      IF(F1.LT..5) GO TO 999
      PRINT 300,NO
  300 FORMAT(//* HOLOGRAM NUMBER *I5)
    2 DO 3 I=1,N
    3 P(I)=P(I)*1.75E-5
      F2=T1*1.57074635*Z*RO/(T2*W*W*DA*SL)
   10 X=-DX
      DO4I=1,N
      X=X+DX
      XI(I)=X-10.
      XL=BL-X
      TH=ATAN2(X,XL)
    4 DENS(I)=P(I)*F2*XL/(PRF*COS(TH))
C  PRINT FINAL RESULTS ONLY
      IF(F1-1.1)12,12,11
   11 WRITE(6,100)F2,(XI(I),DENS(I),I=1,N)
      GO TO 1
C  NORMALIZE TO TRANSMISSION MEASUREMENT
   12 SUM=0.
      NN=N-1
      DO5J=1,NN
    5 SUM=SUM+DENS(I)+DENS(I+1)
      BN1=SUM*DX/(2*BL)
      BN2=-ALOG(T2/T1)/(SL*BL)
      WRITE(6,200)BN1,BN2
  200 FORMAT(//* BN1 = *E15.8*  BN2 = *E15.8///)
      F1=2.
      F2=F2*BN2/BN1
      GO TO 10
  100 FORMAT(/* F2 = *E15.8//* X(INCHES)  DENSITY*//(F5.1,5X,E10.3))
  999 STOP
      END
```

Figure B-1 (continued)

```
  $INP
?  NØ=1781,T1=18.,T2=14.,DX=3.,N=32,P=.045,.06,.05,.055,.055,.05,.055,
?  .055,.05,.05,.055,.06,.065,.075,.075,.076,.078,.08,.075,.065,.085,
?  .085,.072,.09,.075,.1,.08,.1,.068,.115,.085,.065$

 HØLØGRAM NUMBER  1781

 BN1 =  8.46797146E+05  BN2 =  1.63712089E+06


 F2 =  4.00372011E+10

 X(INCHES)  DENSITY

-10.0       4.067E+06
 -7.0       5.298E+06
 -4.0       4.314E+06
 -1.0       4.637E+06
  2.0       4.532E+06
  5.0       4.028E+06
  8.0       4.333E+06
 11.0       4.240E+06
 14.0       3.773E+06
 17.0       3.696E+06
 20.0       3.986E+06
 23.0       4.268E+06
 26.0       4.542E+06
 29.0       5.154E+06
 32.0       5.077E+06
 35.0       5.074E+06
 38.0       5.146E+06
 41.0       5.224E+06
 44.0       4.856E+06
 47.0       4.182E+06
 50.0       5.446E+06
 53.0       5.434E+06
 56.0       4.603E+06
 59.0       5.766E+06
 62.0       4.826E+06
 65.0       6.475E+06
 68.0       5.224E+06
 71.0       6.597E+06
 74.0       4.540E+06
 77.0       7.784E+06
 80.0       5.842E+06
 83.0       4.542E+06
```

Figure B-1 (continued)

```
  $INP
?  NØ=1782,T2=15.,P=.01,.02,.02,.03,.035,.04,.04,.04,.04,.04,.045,.055,
?  .07,.08,.075,.093,.085,.06,.065,.065,.065,.08,.125,.205,.22,
?  .22,.123,.093,.105,.15,.07,.06$

 HØLØGRAM NUMBER  1782

 BN1 =  7.29548311E+05  BN2 =  1.18768521E+06


 F2 =  3.14663532E+10

 X(INCHES)  DENSITY

-10.0       7.104E+05
 -7.0       1.388E+06
 -4.0       1.356E+06
 -1.0       1.988E+06
  2.0       2.267E+06
  5.0       2.533E+06
  8.0       2.477E+06
 11.0       2.423E+06
 14.0       2.372E+06
 17.0       2.324E+06
 20.0       2.563E+06
 23.0       3.074E+06
 26.0       3.844E+06
 29.0       4.321E+06
 32.0       3.990E+06
 35.0       4.880E+06
 38.0       4.407E+06
 41.0       3.079E+06
 44.0       3.308E+06
 47.0       3.287E+06
 50.0       3.273E+06
 53.0       4.019E+06
 56.0       6.280E+06
 59.0       1.032E+07
 62.0       1.112E+07
 65.0       1.120E+07
 68.0       6.312E+06
 71.0       4.822E+06
 74.0       5.510E+06
 77.0       7.980E+06
 80.0       3.781E+06
 83.0       3.295E+06
```

Figure B-1 (continued)

```
  $INP
?  NØ=1783,T2=11.,P=.01,.03,.04,.05,.07,.11,.13,.13,.136,.15,.152,.16,.17,
?  .19,.196,.18,.18,.17,.19,.196,.206,.214,.23,.244,.27,.27,.286,
?  .21,.252,.31,.17,.15$

 HØLØGRAM NUMBER  1783

 BN1 =  2.48709651E+06  BN2 =  3.20810687E+06


 F2 =  3.39980402E+10

 X(INCHES)  DENSITY

-10.0       7.675E+05
 -7.0       2.250E+06
 -4.0       2.931E+06
 -1.0       3.580E+06
  2.0       4.898E+06
  5.0       7.525E+06
  8.0       8.698E+06
 11.0       8.510E+06
 14.0       8.715E+06
 17.0       9.416E+06
 20.0       9.355E+06
 23.0       9.664E+06
 26.0       1.009E+07
 29.0       1.109E+07
 32.0       1.127E+07
 35.0       1.021E+07
 38.0       1.008E+07
 41.0       9.426E+06
 44.0       1.045E+07
 47.0       1.071E+07
 50.0       1.121E+07
 53.0       1.162E+07
 56.0       1.249E+07
 59.0       1.327E+07
 62.0       1.475E+07
 65.0       1.485E+07
 68.0       1.586E+07
 71.0       1.176E+07
 74.0       1.429E+07
 77.0       1.782E+07
 80.0       9.921E+06
 83.0       8.900E+06
```

Figure B-1 (continued)

```
 $INP
?  N0=1784,T2=13.,P=.11,.13,.13,.15,.176,.19,.2,.19,.16,.14,.124,.13,.15,
?  .15,.14,.16,.172,.18,.164,.17,.204,.174,.18,.246,.324,.35,.39,
?  .372,.41,.42,.11,.06$

 HØLØGRAM NUMBER  1784

 BN1 =  8.41786512E+05  BN2 =  2.11987754E+06


 F2 =  5.61637163E+10

 X(INCHES)  DENSITY

-10.0       1.395E+07
 -7.0       1.610E+07
 -4.0       1.573E+07
 -1.0       1.774E+07
  2.0       2.035E+07
  5.0       2.147E+07
  8.0       2.210E+07
 11.0       2.055E+07
 14.0       .694E+07
 17.0       1.452E+07
 20.0       1.261E+07
 23.0       1.297E+07
 26.0       1.470E+07
 29.0       1.446E+07
 32.0       1.329E+07
 35.0       1.499E+07
 38.0       1.592E+07
 41.0       1.649E+07
 44.0       1.490E+07
 47.0       1.534E+07
 50.0       1.833E+07
 53.0       1.560E+07
 56.0       1.614E+07
 59.0       2.211E+07
 62.0       2.924E+07
 65.0       3.179E+07
 68.0       3.572E+07
 71.0       3.443E+07
 74.0       3.840E+07
 77.0       3.988E+07
 80.0       1.060E+07
 83.0       5.881E+06
```

APPENDIX C

AEROSOL DROPLET DENSITY
APPENDIX C

SCATTER CHAMBER
VOL. = $V_c \sim 24{,}000$ IN^3

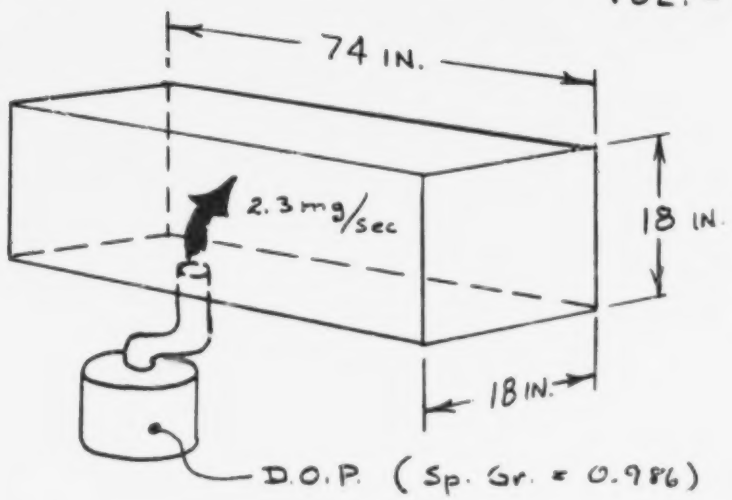

PARTICLE VOL. AND WEIGHT

Assume a monodisperse aerosol with particle diameter of 0.69 μ

$$D_p = 0.69\mu \times 0.394 \times 10^{-4}\ \text{IN}/\mu = 0.272 \times 10^{-4}\ \text{IN.}$$

$$V_p = \frac{1}{6}\pi D^3 = \frac{3.14}{6}(0.272 \times 10^{-4})^3 \simeq 0.01 \times 10^{-12}\ \text{IN.}^3$$

$$\rho_p \approx \rho_{H_2O} = 0.036\ \text{Lb/IN}^3$$

$$W_p = \rho V_p = 0.036\ \text{Lb/IN}^3 \times 0.01 \times 10^{-12}\ \text{IN}^3$$

$$W_p = 0.036 \times 10^{-14}\ \text{Lb.}$$

TOTAL NUMBER OF PARTICLES IN CHAMBER

D.O.P. was injected into the chamber for a duration of 10 sec. at a rate of 2.3 mg/sec.

$$W_{total} = \dot{w} \times t = 2.3 \times 10^{-3}\ \text{g/sec} \times 10\ \text{sec}$$

$$= 23 \times 10^{-3}\ \text{g}$$

AEROSOL DROPLET DENSITY APPENDIX C

$W_{total} = 23 \times 10^{-3}\ g \times 2.205\ Lb/g = 5.07 \times 10^{-5}\ Lb\ D.O.P.$ IN 10 sec.

$$Vol._{Total} = \frac{W_{total}}{\rho_{DOP}} = \frac{5.07 \times 10^{-5}\ Lb}{0.036\ Lb/IN^3} = 140.8 \times 10^{-5}\ IN.^3$$

Number of particles in chamber = N_t

$$N_t = \frac{Vol._{total\ (D.O.P.)}}{V_p} = \frac{140.8 \times 10^{-5}\ IN.^3}{0.01 \times 10^{-12}\ IN.^3}$$

$N_t \simeq 1.4 \times 10^{11}$ Particles

PARTICLE DENSITY

$$Density = \frac{N_t}{V_c} = \frac{1.4 \times 10^{11}\ Particles}{24 \times 10^3\ IN.^3}$$

$= 5.8 \times 10^6$ Particles / IN.^{3}

= 5.8 million particles / cubic inch

Ideally, with a second 10 sec. injection of D.O.P. at the same flow rate, no losses, etc, the particle density would have been $= 11.6 \times 10^6$ part. / IN.^{3}